JOURNAL OF PETROLOGY | VOLUME 47 | NUMBER 8 | PAGES 1557–1589 | 2006 | doi:10.1093/petrology/egl020

# Petrology and Geochemistry of the Quaternary Caldera-forming, Phonolitic Granadilla Eruption, Tenerife (Canary Islands)

**SCOTT E. BRYAN***

DEPARTMENT OF GEOLOGY & GEOPHYSICS, YALE UNIVERSITY, PO BOX 208109 NEW HAVEN, CT 06520-8109, USA

**RECEIVED JUNE 20, 2005; ACCEPTED MARCH 15, 2006; ADVANCE ACCESS PUBLICATION APRIL 9, 2006**

*The Granadilla eruption at 600 ka was one of the largest phonolitic explosive eruptions from the Las Cañadas volcano on Tenerife, producing a classical plinian eruptive sequence of a widespread pumice fall deposit overlain by an ignimbrite. The eruption resulted in a major phase of caldera collapse that probably destroyed the shallow-level magma chamber system. Granadilla pumices contain a diverse phenocryst assemblage of alkali feldspar + biotite + sodian diopside to aegirine–augite + titanomagnetite + ilmenite + nosean/haüyne + titanite + apatite; alkali feldspar is the dominant phenocryst and biotite is the main ferromagnesian phase. Kaersutite and partially resorbed plagioclase (oligoclase to sodic andesine) are present in some eruptive units, particularly in pumice erupted during the early plinian phase, and in the Granadilla ignimbrite at the top of the sequence. Associated with the kaersutite and plagioclase are small clots of microlitic plagioclase and kaersutite interpreted as quenched blebs of tephriphonolitic magma within the phonolite pumice. The Granadilla Member has previously been recognized as an example of reverse-then-normal compositional zonation, where the zonation is primarily expressed in terms of substantial variations in trace element abundances with limited major element variation (cryptic zonation). Evidence for cryptic zonation is also provided by the chemistry of the phenocryst phases, and corresponding changes in intensive parameters (e.g.* $T$, $fO_2$, $fH_2O$*). Geothermometry estimates indicate that the main body of phonolite magma had a temperature gradient from* $860^\circ C$ *to* $\sim 790^\circ C$*, with hotter magma (*$\geq 900^\circ C$*) tapped at the onset and terminal phases of the eruption. The reverse-then-normal chemical and thermal zonation reflects the initial tapping of a partially hybridized magma (mixing of phonolite and tephriphonolite), followed by the more sequential tapping of a zoned and relatively large body of highly evolved phonolite at a new vent and during the main plinian phase. This suggests that the different magma types within the main holding chamber could have been laterally juxtaposed, as well as in a density-stratified arrangement. Correlations between the presence of mixed phenocryst populations (i.e. presence of plagioclase and kaersutite) and coarser pumice fall layers suggest that increased eruption vigour led to the tapping of hybridized and/or less evolved magma probably from greater depths in the chamber. New oxygen isotope data for glass and mineral separates preclude syn-eruptive interaction between the vesiculating magma and hydrothermal fluids as the cause of the Sr isotope disequilibrium identified previously for the deposit. Enrichment in radiogenic Sr in the pumice glass has more likely been due to low-temperature exchange with meteoric water that was enriched in* $^{87}Sr$ *by sea spray, which may be a common process affecting porous and glassy pyroclastic deposits on oceanic islands.*

KEY WORDS: *zoned magma chamber; explosive eruption; oxygen isotopes; phonolite; plinian; Tenerife*

## INTRODUCTION

An extensive succession of Quaternary phonolitic pyroclastic deposits is preserved along the southern coast of Tenerife. These are the products of many explosive eruptions from the Las Cañadas volcano (Fig. 1) between ~1·6 and 0·17 Ma (Martí *et al.*, 1994; Bryan *et al.*, 1998*a*). These explosive eruptions produced extensive plinian fall deposits and/or ignimbrites, and at least four eruptions culminating in summit caldera collapse have now been recognized over the last 600 kyr (Bryan *et al.*, 1998*a*, 1998*b*, 2001; Edgar *et al.*, 2002; Brown *et al.*, 2003). This recent period of explosive

*Present address: School of Earth Sciences and Geography, Kingston University, Penrhyn Road, Kingston upon Thames KT1 2EE, UK. Telephone: +44 (0)20 8547 7084. Fax.: +44 (0)20 8547 7497. E-mail: S.Bryan@kingston.ac.uk

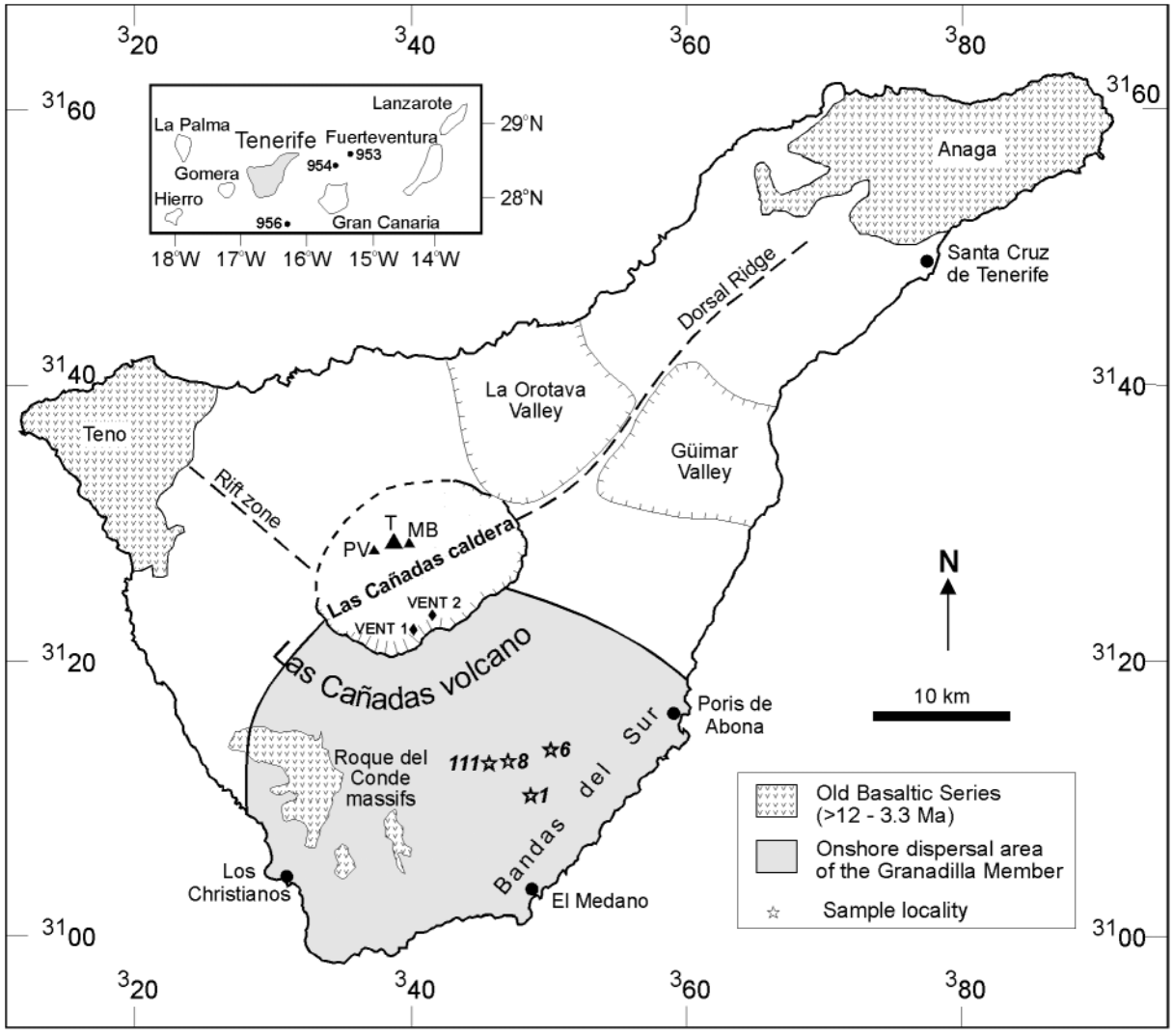


**Fig. 1.** Map of Tenerife showing the location of Las Cañadas volcano and its nested summit caldera containing the post-170 ka stratovolcanic complex of Teide (T), Pico Viejo (PV) and Montaña Blanca (MB); the major sector collapse scars (the Güimar and La Orotava valleys); and the Bandas del Sur, where an extensive Quaternary phonolitic pyroclastic succession is preserved. The onshore dispersal area of the Granadilla Member is shown along with locations of the two inferred vents within the caldera for the eruption (Bryan *et al.*, 2001). Stars and italicized numbers are sample locations of the Granadilla Member. The numbered grid represents 20 km intervals of the UTM grid, zone 28 for the northern hemisphere. Inset map shows the location of Tenerife within the Canary Islands and the offshore drill sites (Ocean Drilling Program Leg 157, sites 953, 954 and 956) where deposits from the Las Cañadas volcano have been reported, and a 610 ± 20 ka ash in hole 953 may be distal deposits from the Granadilla eruption (Brown *et al.*, 2003).

volcanism and caldera collapse followed construction of the large basaltic to phonolitic Las Cañadas shield volcano between >3·3 Ma and 2 Ma (Martí *et al.*, 1994), which superseded earlier basaltic shield-building volcanism during the Miocene and Pliocene (~12–3·3 Ma; Old Basaltic Series of Fuster *et al.*, 1968; Ancochea *et al.*, 1990; Thirlwall *et al.*, 2000).

Several recent studies (Bryan *et al.*, 1998*a*, 2002; Edgar *et al.*, 2002; Brown *et al.*, 2003) have highlighted the stratigraphical and geochemical characteristics of the young (<600 ka) pyroclastic deposits of the Las Cañadas volcano, which share the following characteristics: (1) they are interbedded with basaltic lavas; (2) they have eruptive stratigraphies with complex alternations between plinian fall, pyroclastic density current and also, commonly, phreatomagmatic fall and density current deposits; (3) they contain banded pumice and mixed phenocryst assemblages; and (4) abundant syenite clasts are present in lithic breccia facies of the ignimbrites. In contrast, several explosive eruptions ≥600 ka produced deposits with the more classical plinian eruptive stratigraphy of widespread fall deposits (reflecting the establishment of a buoyant eruption column) followed by ignimbrites, which represent column collapse

(Booth, 1973; Bryan *et al.*, 1998*a*; Brown *et al.*, 2003). Furthermore, some of these older plinian deposits exhibit an 'occult' or 'cryptic' chemical zonation (Wolff & Storey, 1984; Bryan *et al.*, 2002), lacking demonstrable evidence from outcrop features for chemical zonation or magma heterogeneity (e.g. banded pumice, mixed phenocryst assemblages). The best described example of a plinian deposit with cryptic compositional zonation is the widespread Granadilla Member (Bryan *et al.*, 1998*a*, 2001), which arguably represents the largest volume explosive eruption of a relatively homogeneous phonolitic magma body at Tenerife. The Granadilla eruption, however, was unusual in that the plinian fall deposits show a reverse-then-normal cryptic compositional zonation up sequence (Wolff & Storey, 1984; Bryan *et al.*, 1998*a*). The aim of this paper then is to present a comprehensive mineral chemistry and whole-rock geochemical dataset, based on detailed stratigraphic sampling of the Granadilla Member, to constrain: (1) the nature of the pre-eruptive magma system; (2) the extent to which fractional crystallization (Wolff & Palacz, 1989), magma mixing, or crustal assimilation were important in determining the evolution of the magma body; and (3) the effects of withdrawal dynamics on pumice geochemistry.

## The Granadilla eruption

The deposit characteristics and reconstruction of the Granadilla eruption have been detailed by Bryan *et al.* (2001). This eruption produced one of the most widely dispersed and largest volume pyroclastic units on Tenerife (Fig. 1) and culminated in a major episode of caldera collapse at 600 ± 7 ka, based on the new $^{40}Ar/^{39}Ar$ age constraints of Brown *et al.* (2003). This episode of caldera collapse was followed by a significant hiatus in major phonolitic explosive volcanism of possibly up to ~250 kyr, with the caldera-forming Fasnia eruption at 289 ± 6 ka (Brown *et al.*, 2003). The shallow-level magma chamber beneath the Las Cañadas caldera was probably destroyed by caldera collapse during the Granadilla eruption, resulting in a considerable period of time before a new shallow-level chamber was re-established in the eastern sector of the caldera (Martí *et al.*, 1994; Bryan *et al.*, 1998*a*).

The eruption produced a plinian fall deposit (Granadilla pumice of Booth, 1973) that is up to 9 m thick at ~10 km downwind of the caldera (location 8, Fig. 1) and at its nearest preserved full exposure to the Las Cañadas caldera. The fall deposit has been divided into four main units (Fig. 2), with Unit 2 a thin, but distinctive ash fall layer (~2 cm thick) of phreatoplinian origin (Bryan *et al.*, 2001). The lithic-rich nature and abundance of unaltered lithic fragments within Unit 2 have been interpreted to reflect magma interaction with aquifer-derived water at depth (Bryan *et al.*, 2001). Unit 3 (≤1·8 m thick) records a reversal to dry plinian eruptive activity, and Unit 4, the thickest and most widely dispersed fall unit (up to 6·3 m thick at 10 km from vent), records the maximum dispersal and intensity of the eruption. Covering Unit 4 is the widespread (>500 $km^2$), nonwelded and pumice-rich Granadilla ignimbrite (Unit 5), which records the collapse of a 25–30 km high plinian eruption column (Bryan *et al.*, 2001). A fine-grained vitric ash layer intersected in an offshore drill hole ~150 km to the ENE of Tenerife and dated at 610 ± 20 ka (Bogaard, 1998) has been correlated with the Granadilla eruption based on the similarity in age (Brown *et al.*, 2003), and may represent either distal plinian ash fall or co-ignimbrite ash. A coarse, vent-derived lithic breccia horizon towards the top of the ignimbrite is interpreted to record the onset of caldera collapse late in the eruption (Bryan *et al.*, 1998*b*). Eruption of the Granadilla magma is interpreted to have occurred from two major vents ~1·5 km apart on the SE side of the caldera (Fig. 1), with a shift in vent location occurring between deposition of Units 1 and 3, based on corresponding changes in isopach and isopleth maps for the component fall units (Bryan *et al.*, 2001).

## Previous geochemical studies

Previously published geochemical data show that all the Tenerife phonolitic pyroclastic deposits are geochemically similar, and that fractional crystallization (involving the observed phenocryst assemblages) has been the dominant process in the production of the phonolitic magmas (e.g. Wolff, 1984; Wolff & Storey, 1984; Palacz & Wolff, 1989; Bryan *et al.*, 2002). Major and trace element and isotopic data for the Granadilla Member published by Wolff (1984), Wolff & Storey (1984) and Palacz & Wolff (1989) showed that the central portions of the Granadilla pumice [plinian fall Units 3 and base of Unit 4 of Bryan *et al.* (2001); see Fig. 2] are the most evolved. The base of the Granadilla pumice is geochemically anomalous, showing enrichment in compatible elements such as Ba, Sr, CaO, $P_2O_5$ and $TiO_2$ (Wolff, 1983; Wolff & Storey, 1984; Palacz & Wolff, 1989). Compatible element (Eu, La, Sm, Nd, Ti, P, Sr and Ba) abundances increase and incompatible element (Zr, Nb, Tb, U, Hf, Th, Y, Rb, and Yb) abundances decrease from the evolved central part to the upper part of the deposit (top of Unit 4 and overlying Granadilla ignimbrite). Wolff (1983) suggested that the less evolved upper part was related to the central part of the deposit by simple crystal fractionation. The base and top of the Granadilla Member are similar in composition, although the base shows higher abundances of Eu, CaO, $P_2O_5$, Sr and Ba (Wolff & Storey, 1984). The higher compatible element abundances at the base (Unit 1) were thought to be due to contamination with more mafic country rock and the sampling of less evolved

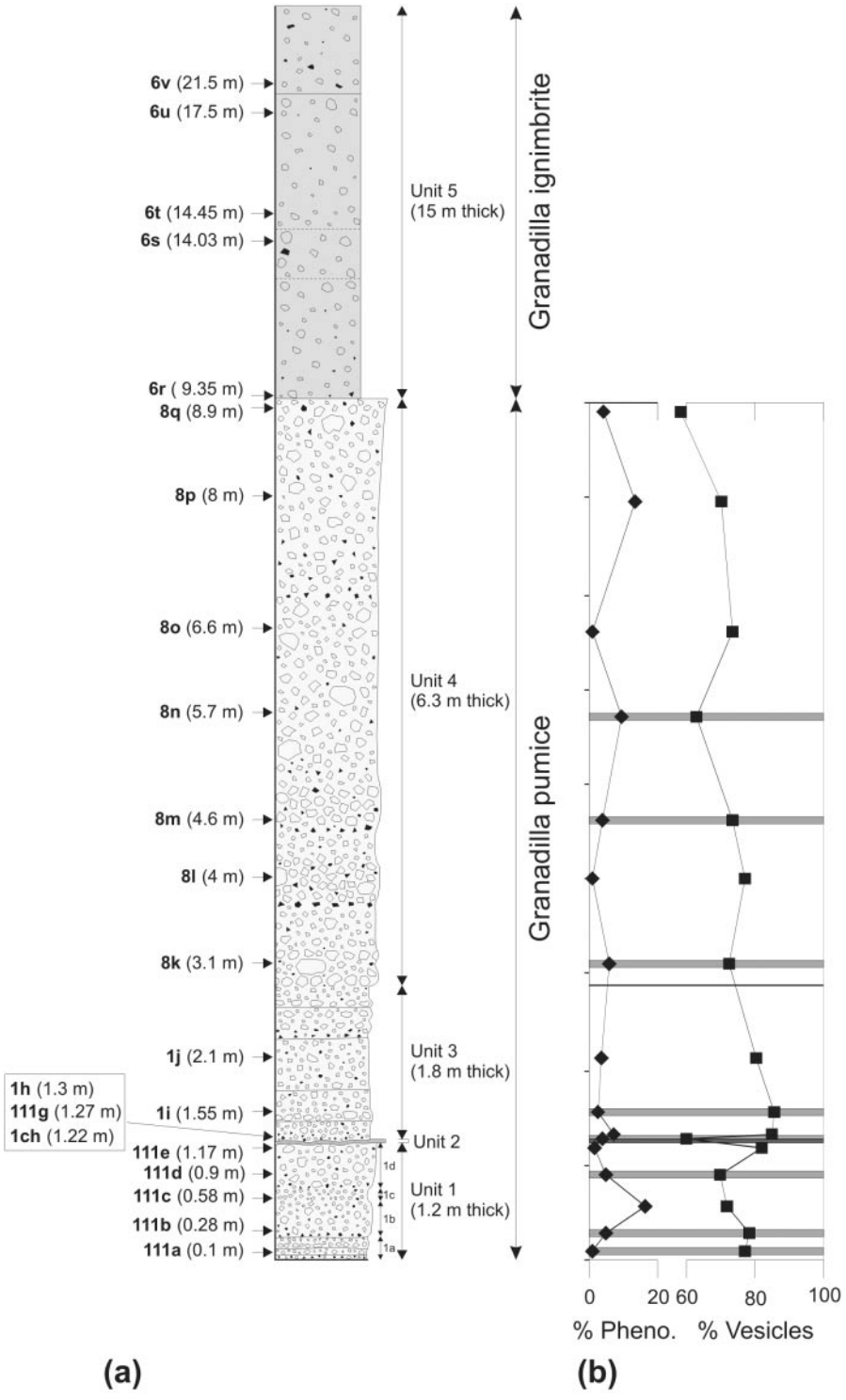


**Fig. 2.** (a) Sample stratigraphy for the Granadilla Member, showing sample heights (in parentheses) of sample numbers (in bold) referred to in text and figures. Numeric prefixes to sample numbers correspond to sample locations shown in Fig. 1. (b) Modal data for the Granadilla pumice samples (see Table 1); Pheno., phenocrysts. Continuous lines denote fall unit boundaries, and horizontal grey bars denote sample horizons where tephriphonolitic magma components (microcrystalline kaersutite and plagioclase glass blebs with microcrystalline kaersutite and plagioclase, and/or glass containing plagioclase, kaersutite, Mg- and Al-rich Fe-Ti oxide phenocrysts) are present. Bulk-pumice vesicularity is reduced where tephriphonolitic glass is present; however, the overall trend is for increasing pumice vesicularity from Unit 1 to Unit 3 (maximum vesicularity of 86%), then a decrease to the top of Unit 4. Granadilla pumices are mostly phenocryst-poor (<10 modal %).

*Table 1: Modal data for Granadilla pumice samples based on 1000 optical point counts of thin sections*

| Sample: | 111a | 111b | 111c | 111d | 111e | 111g | 1h | 1i | 1j | 8k | 8l | 8m | 8n | 8o | 8p | 8q |
|---|---|---|---|---|---|---|---|---|---|---|---|---|---|---|---|---|
| Sample height (m): | 0·08 | 0·28 | 0·58 | 0·9 | 1·17 | 1·27 | 1·3 | 1·55 | 2·12 | 3·1 | 4 | 4·6 | 5·72 | 6·6 | 7·98 | 8·9 |
| Unit: | 1 | 1 | 1 | 1 | 1 | 3 | 3 | 3 | 3 | 4 | 4 | 4 | 4 | 4 | 4 | 4 |
| *Percentage* | | | | | | | | | | | | | | | | |
| Vesicle | 77 | 78 | 72 | 70 | 82 | 60 | 85 | 86 | 80 | 72 | 77 | 74 | 63 | 74 | 70 | 58 |
| Pumice glass | 23 | 20 | 23 | 29 | 18 | 38 | 14 | 14 | 19 | 26 | 23 | 25 | 32 | 26 | 26 | 40 |
| Alkali feldspar | <1 | 1 | 3 | 1 | <1 | 2 | 1 | <0·1 | <1 | 2 | <0·1 | 1 | 3 | <1 | 4 | 1 |
| Plagioclase | tr | <1 | 1 | tr | — | tr | — | tr | — | tr | — | — | tr | — | — | — |
| Biotite | — | <0·1 | 1 | <1 | <0·1 | <0·1 | <0·1 | <1 | <0·1 | <0·1 | <0·1 | <0·1 | <0·1 | <0·1 | <0·1 | <1 |
| Kaersutite | — | <0·1 | tr | <0·1 | — | <0·1 | — | — | — | — | — | — | — | — | — | — |
| Pyroxene | — | tr | — | tr | tr | tr | — | <0·1 | — | <0·1 | — | <0·1 | <1 | tr | — | tr |
| Fe–Ti oxide | — | <0·1 | 0 | <0·1 | tr | tr | <1 | <0·1 | <0·1 | — | tr | <0·1 | <0·1 | <0·1 | tr | tr |
| Titanite | — | tr | tr | <0·1 | — | tr | — | <0·1 | <1 | — | — | tr | <1 | tr | tr | <1 |
| Haüyne | — | — | — | — | — | — | — | tr | — | — | tr | tr | — | — | tr | — |
| Microcryst. glass bleb | <0·1 | 1 | <1 | <0·1 | — | 1 | — | — | <0·1 | <1 | — | — | 1 | — | — | — |
| Phenocrysts | 1 | 5 | 16 | 5 | 2 | 4 | 7 | 3 | 4 | 6 | 1 | 4 | 9 | 1 | 13 | 4 |
| Groundmass | 99 | 95 | 84 | 95 | 98 | 96 | 93 | 97 | 96 | 94 | 99 | 96 | 91 | 99 | 87 | 96 |
| Vesicles | 77 | 78 | 72 | 70 | 82 | 60 | 85 | 86 | 80 | 72 | 77 | 74 | 63 | 74 | 70 | 58 |

Total phenocryst content is vesicle free, and groundmass is pumice glass that only rarely contains feldspar microlites. Microcryst. glass bleb, tephriphonolitic glass bleb comprising fine-grained intergrowths of kaersutite, plagioclase, Fe–Ti oxides ± apatite (see Fig. 6a); tr, trace amount—phase is present in sample but not counted. Pumice vesicularities are close to the generally accepted 'fragmentation vesicularity' threshold of 75–83% (Sparks, 1978) and similar to the bulk vesicularity of pumices observed for calc-alkaline plinian explosive eruptions (e.g. Thomas *et al.*, 1994). Bulk-pumice vesicularity is lower where tephriphonolitic glass is present in the sample (e.g. samples 111g and 8n).

magma at the onset of the eruption (Wolff & Storey, 1984; Palacz & Wolff, 1989).

The Granadilla eruption is also significant because it has been described as an example of interaction between a vesiculating magma and hydrothermal fluids with high $^{87}Sr/^{86}Sr$ in the conduit, immediately prior to, and/or during, explosive eruption (Palacz & Wolff, 1989). The evidence for this model was based on variations in bulk-pumice $^{87}Sr/^{86}Sr$ ratios, in which the pumice glasses have the most radiogenic strontium isotope compositions, whereas the feldspar phenocrysts have no Sr isotopic enrichment, with $^{87}Sr/^{86}Sr$ isotopic values of 0·7031–0·7032, identical to Tenerife basaltic magmas (Palacz & Wolff, 1989). Similar Sr isotopic disequilibrium between phenocrysts and glass has been described from silicic ignimbrites on neighbouring Gran Canaria (Cousins *et al.*, 1993), suggesting this may be a common feature of the silicic rocks in the Canary Islands.

In summary, previous studies have shown that the Granadilla Member exhibits complex vertical chemical variations in major, trace element, and Nd–Sr isotope characteristics, suggesting that the eruption did not proceed via single-stage draw-down of a simple, zoned magma chamber. Despite the published whole-rock chemistry on the Granadilla Member, no phenocryst chemistry data [except for one titanite phenocryst analysis by Wolff (1984)] have been published. The whole-rock chemistry of volcanic rocks typically represents the cumulative effects of magmatic processes such as fractional crystallization and magma mixing, whereas a detailed study of the phenocryst phase chemistry and zonation patterns can be particularly insightful in providing an important record of pre-eruptive magma interactions and processes, and a better characterization of the magma end-members involved.

## SAMPLE SELECTION AND ANALYTICAL METHODS

The complete mineral, glass, and whole-rock geochemical datasets can be downloaded from the *Journal of Petrology* website at: http://www.petrology.oupjournals.org. Sample locations referred to in this paper and the geochemical datasets are based on zone 28 of the Universal Transverse Mercator grid for the northern hemisphere (WGS84 datum). The relative stratigraphy and sample numbers for the Granadilla Member referred to in the text and figures are shown in Fig. 2. Modal data for Granadilla pumice samples are summarized in Table 1.

## Sampling methods

Pumice clasts represent quenched portions of vesiculated magma, and chemical and petrographic variations between pumices record variations in the magma chamber that were frozen at the time of eruption (Hildreth, 1981). The Granadilla pumice was sampled at three localities, each representing the maximum thickness of the three plinian pumice fallout units. Isopach maps for the component fallout units (see Bryan *et al.*, 2001) show that the axes of dispersal do not overlap, such that sampling based on the total deposit thickness will not accurately record the full geochemical variation. In places, the pumice has undergone patchy calcite cementation, and visibly affected pumices were not sampled. Sampling of the Granadilla pumice follows the method recommended by Wolff (1985) where the coarsest pumice clasts at each sampling level were collected for analysis.

For studies of ignimbrite geochemistry, the analysis of fresh pumices is preferable to whole-rock samples. Syn- and post-eruptive processes such as ash elutriation during transport (crystal-enrichment; Walker, 1972), incorporation of vent- and locally derived lithic fragments, and devitrification and vapour-phase alteration following deposition can obscure original magmatic variations (Hildreth & Mahood, 1985). A section through the Granadilla ignimbrite was sampled where the ignimbrite was relatively thick (~16 m) to identify any overall vertical compositional variation. The ignimbrite, however, has had a complex post-eruptive history that has significantly modified the bulk sample chemistry and any primary compositional zonation that may have been present. Physical mixing and abrasion of the juvenile particles (pumice and ash) have occurred during transport by the highly turbulent pyroclastic density currents [particulate mixing of Sumner & Wolff (2003)]. Deposit features such as erosional surfaces, and the complete removal of the underlying Granadilla pumice at some locations (Bryan, 1998; Bryan *et al.*, 2001), show that the Granadilla ignimbrite geochemistry has been compromised by the incorporation, via substrate erosion, of pre-existing and chemically heterogeneous deposits. Most of the Granadilla ignimbrite has undergone vapour-phase alteration, lithifying the vitriclastic ash matrix but altering pumice clasts to clays or zeolites (e.g. Pérez-Torrado *et al.*, 1995). At the sampling location, the ignimbrite is mostly vapour-phase altered, which is reflected in scattered MgO, CaO and alkali contents and in particular, elevated Ba and Sr contents (see Table 2). Only the topmost ignimbrite bed at the sampling location has been unaffected by vapour-phase alteration. Consequently, an inaccurate record of geochemical variation is given by the ignimbrite samples.

## Analytical techniques

### *X-ray fluorescence*

For the Granadilla pumice samples, 2–4 pumice clasts of similar dimensions were lightly crushed using only a tungsten carbide concentric ring (tema) mill where the clast size was small enough (e.g. Unit 1), or a primary jaw crusher to first reduce clast size. Two-stage crushing (jaw crushing followed by tungsten carbide tema mill) was required for whole-rock ignimbrite samples. Any visible lithic fragments were removed from ignimbrite samples prior to milling, and any remaining contaminating lithic fragments were also removed prior to tema milling. Some ash loss, especially for pumice samples, was unavoidable during both crushing stages.

Major and trace element concentrations were determined at the Department of Earth Sciences, University of Queensland, by X-ray fluorescence spectrometry (XRF) using a Philips PW1400 wavelength-dispersive X-ray spectrometer, Philips PW1730 60 kV X-ray generator, Philips PW1500 72 position sample changer, and Rh and Au anode X-ray tubes. Fused discs for major element analysis were prepared by the Norrish & Hutton (1969) method. Pressed pellets (trace element analysis) used an in-house technique similar to those used at the Department of Geochemistry, University of Capetown. All major element XRF data have been normalized to 100% on an anhydrous basis, and trace element data have been normalized on a loss on ignition (LOI)-free basis. LOI was determined by weight loss after drying sample powders in an oven. Approximately 1–1·5 g of sample in a preweighed ceramic crucible was heated overnight at 105 °C and reweighed. The samples were then heated to 800 °C for 2–3 h, then reweighed when cool. At higher temperatures, the phonolite powders fused. Fused discs were then prepared from the ignited powders.

### *Inductively coupled plasma-mass spectrometry (ICP-MS)*

Selected samples were analysed for trace and rare earth elements (REE) by inductively coupled plasma-mass spectrometry (ICP-MS) at the Department of Earth Sciences, Monash University. Powders were prepared using an agate concentric ring mill. Aliquots (100 mg) of each sample were digested for 24–48 h in Savillex-type teflon bombs at 150 °C in a mixture of distilled HF (3 ml) and $HNO_3$ (1 ml). Sample solutions were dried in HEPA-filtered clean air cabinets, followed by conversion of fluorides to nitrates with two additions of concentrated $HNO_3$. Samples were then taken into solution with 50 g of 2·5% $HNO_3$ (made up with sub-boiled distilled concentrated $HNO_3$ and 18·2 Mohm Millipore water). All samples were also made up to 100 ppb indium to serve as an internal standard to correct for instrument drift. One analytical blank and at least three standard

*Table 2: Major and trace element data for bulk-pumice samples from the Granadilla pumice (Units 1–4), and bulk ignimbrite samples from the Granadilla ignimbrite (Unit 5)*

| Sample: | 111a | 111b | 111c | 111d | 111e | 111g | 1h | 1i | 1j | 8k |
|---|---|---|---|---|---|---|---|---|---|---|
| Eruptive unit: | 1 | 1 | 1 | 1 | 1 | 3 | 3 | 3 | 3 | 4 |
| Sample height (m): | 0·08 | 0·28 | 0·58 | 0·9 | 1·17 | 1·27 | 1·3 | 1·55 | 2·12 | 3·1 |
| Easting: | 346·406 | 346·406 | 346·406 | 346·406 | 346·406 | 346·406 | 349·39 | 349·39 | 349·39 | 347·76 |
| Northing: | 3111·71 | 3111·71 | 3111·71 | 3111·71 | 3111·71 | 3111·71 | 3109·387 | 3109·387 | 3109·387 | 3111·823 |
| *Major elements (wt %)* | | | | | | | | | | |
| $SiO_2$ | 61·22 | 61·16 | 61·05 | 60·91 | 61·13 | 61·08 | 61·07 | 61·01 | 60·84 | 61·10 |
| $TiO_2$ | 0·66 | 0·60 | 0·55 | 0·53 | 0·52 | 0·50 | 0·51 | 0·52 | 0·51 | 0·49 |
| $Al_2O_3$ | 19·42 | 19·59 | 19·86 | 19·71 | 19·73 | 19·88 | 19·97 | 20·07 | 19·99 | 19·97 |
| $Fe_2O_3T$ | 3·38 | 3·31 | 3·38 | 3·38 | 3·39 | 3·39 | 3·45 | 3·43 | 3·45 | 3·40 |
| MnO | 0·23 | 0·24 | 0·25 | 0·26 | 0·26 | 0·27 | 0·27 | 0·27 | 0·28 | 0·27 |
| MgO | 0·92 | 0·56 | 0·47 | 0·60 | 0·63 | 0·66 | 0·53 | 0·53 | 0·51 | 0·51 |
| CaO | 0·97 | 0·83 | 0·78 | 0·77 | 0·75 | 0·71 | 0·74 | 0·74 | 0·70 | 0·68 |
| $Na_2O$ | 7·25 | 7·44 | 7·54 | 7·83 | 7·56 | 7·24 | 7·60 | 7·48 | 7·72 | 7·37 |
| $K_2O$ | 5·88 | 6·19 | 6·06 | 5·94 | 5·97 | 6·22 | 5·84 | 5·90 | 5·97 | 6·17 |
| $P_2O_5$ | 0·08 | 0·07 | 0·06 | 0·06 | 0·06 | 0·05 | 0·04 | 0·05 | 0·04 | 0·04 |
| LOI | 7·05 | 6·93 | 7·30 | 7·27 | 7·55 | 7·79 | 8·39 | 8·48 | 8·37 | 7·73 |
| *Trace elements (ppm)* | | | | | | | | | | |
| Ba | 528 | 257 | 208 | 161 | 139 | 92 | 90 | 141 | 43 | 42 |
| Rb | 223 | 183 | 250 | 199 | 256 | 251 | 206 | 244 | 209 | 250 |
| Sr | 92 | 40 | 43 | 30 | 33 | 26 | 30 | 35 | 19 | 21 |
| Y | 58 | 51 | 60 | 52 | 61 | 58 | 50 | 57 | 51 | 60 |
| Zr | 1330 | 1262 | 1555 | 1434 | 1626 | 1603 | 1502 | 1588 | 1530 | 1681 |
| Nb | 330 | 288 | 366 | 310 | 380 | 370 | 321 | 367 | 325 | 379 |
| Th | 32 | 39 | 40 | 44 | 41 | 36 | 48 | 34 | 48 | 37 |
| U | 9 | 9 | 10 | 11 | 11 | 9 | 11 | 8 | 10 | 9 |
| Pb | 18 | 16 | 20 | 18 | 21 | 21 | 19 | 22 | 18 | 23 |
| Ga | 43 | — | 46 | — | 46 | 44 | — | 44 | — | 45 |
| Zn | 119 | 165 | 130 | 181 | 134 | 127 | 187 | 126 | 187 | 126 |
| Cu | 6 | b.d.l. | 5 | b.d.l. | 5 | 5 | b.d.l. | 7 | b.d.l. | 4 |
| Ni | 3 | 2 | 2 | 2 | 2 | 2 | 6 | 5 | 11 | 3 |
| V | 47 | 38 | 42 | 35 | 39 | 37 | 32 | 37 | 32 | 38 |
| Cr | 3 | 8 | 4 | 7 | 3 | 3 | 8 | 5 | 10 | 3 |
| Hf | 21 | — | 24 | — | 25 | 25 | — | 24 | — | 25 |
| Cs | 3 | — | 3 | — | 3 | 3 | — | 3 | — | 3 |
| Sc | 11 | — | 14 | — | 18 | 14 | — | 16 | — | 17 |
| Ta | 14 | — | 15 | — | 15 | 14 | — | 14 | — | 15 |
| Co | 13 | 11 | 11 | 12 | 9 | 8 | 20 | 7 | 15 | 10 |
| Ge | 3 | — | 3 | — | 2 | 2 | — | 2 | — | 2 |
| La | 146 | 202 | 156 | 211 | 157 | 152 | 213 | 154 | 215 | 159 |
| Ce | 246 | 264 | 255 | 262 | 252 | 241 | 268 | 246 | 273 | 248 |
| Pr | 22 | — | 22 | — | 21 | 20 | — | 20 | — | 20 |
| Nd | 69 | 70 | 65 | 62 | 62 | 59 | 62 | 60 | 62 | 60 |
| Sm | 10 | — | 9 | — | 8 | 8 | — | 8 | — | 8 |
| Eu | 2 | — | 2 | — | 2 | 2 | — | 2 | — | 2 |
| Gd | 9 | — | 9 | — | 8 | 7 | — | 7 | — | 7 |
| Tb | 1 | — | 1 | — | 1 | 1 | — | 1 | — | 1 |
| Dy | 8 | — | 8 | — | 8 | 8 | — | 8 | — | 8 |
| Ho | 2 | — | 2 | — | 2 | 2 | — | 2 | — | 2 |
| Er | 5 | — | 5 | — | 5 | 6 | — | 6 | — | 6 |
| Tm | 1 | — | 1 | — | 1 | 1 | — | 1 | — | 1 |
| Yb | 6 | — | 6 | — | 6 | 6 | — | 6 | — | 6 |
| Lu | 1 | — | 1 | — | 1 | 1 | — | 1 | — | 1 |

*Table 2: continued*

| Sample: | 8l | 8m | 8n | 8o | 8p | 8q | 6r | 6s | 6t | 6u | 6v |
|---|---|---|---|---|---|---|---|---|---|---|---|
| Eruptive unit: | 4 | 4 | 4 | 4 | 4 | 4 | 5 | 5 | 5 | 5 | 5 |
| Sample height (m): | 4 | 4·6 | 5·72 | 6·6 | 7·98 | 8·9 | 9·35 | 14·03 | 14·45 | 17·52 | 21·52 |
| Easting: | 347·76 | 347·76 | 347·76 | 347·76 | 347·76 | 347·76 | 350·874 | 350·874 | 350·874 | 350·874 | 350·874 |
| Northing: | 3111·823 | 3111·823 | 3111·823 | 3111·823 | 3111·823 | 3111·823 | 3112·688 | 3112·688 | 3112·688 | 3112·688 | 3112·688 |
| *Major elements (wt %)* | | | | | | | | | | | |
| $SiO_2$ | 60·83 | 61·14 | 61·05 | 60·96 | 61·58 | 61·53 | 61·21 | 61·14 | 61·45 | 60·37 | 61·58 |
| $TiO_2$ | 0·50 | 0·49 | 0·54 | 0·57 | 0·58 | 0·63 | 0·63 | 0·68 | 0·74 | 0·72 | 0·70 |
| $Al_2O_3$ | 20·06 | 20·03 | 19·86 | 19·39 | 19·19 | 19·59 | 19·35 | 19·70 | 19·48 | 19·18 | 19·60 |
| $Fe_2O_3T$ | 3·43 | 3·39 | 3·42 | 3·35 | 3·22 | 3·21 | 3·20 | 3·38 | 3·37 | 3·32 | 3·48 |
| MnO | 0·27 | 0·27 | 0·26 | 0·24 | 0·23 | 0·22 | 0·22 | 0·22 | 0·21 | 0·20 | 0·22 |
| MgO | 0·47 | 0·54 | 0·53 | 0·77 | 1·43 | 0·69 | 0·82 | 0·72 | 0·66 | 0·84 | 0·58 |
| CaO | 0·72 | 0·67 | 0·71 | 0·74 | 0·73 | 0·79 | 0·96 | 1·04 | 0·88 | 2·58 | 0·87 |
| $Na_2O$ | 7·23 | 6·75 | 6·65 | 7·08 | 6·09 | 6·60 | 6·59 | 6·25 | 8·43 | 8·13 | 6·93 |
| $K_2O$ | 6·43 | 6·68 | 6·94 | 6·85 | 6·92 | 6·70 | 6·99 | 6·80 | 4·72 | 4·61 | 5·96 |
| $P_2O_5$ | 0·05 | 0·05 | 0·04 | 0·04 | 0·04 | 0·05 | 0·04 | 0·06 | 0·06 | 0·05 | 0·07 |
| LOI | 7·61 | 7·77 | 7·35 | 7·56 | 8·06 | 6·76 | 14·83 | 13·65 | 10·26 | 12·41 | 6·94 |
| *Trace elements (ppm)* | | | | | | | | | | | |
| Ba | 78 | 44 | 61 | 75 | 34 | 49 | 149 | 168 | 197 | 172 | 188 |
| Rb | 202 | 252 | 201 | 220 | 179 | 204 | 172 | 183 | 157 | 167 | 176 |
| Sr | 22 | 19 | 17 | 18 | 14 | 16 | 167 | 148 | 124 | 186 | 62 |
| Y | 49 | 59 | 50 | 56 | 53 | 61 | 41 | 45 | 44 | 47 | 51 |
| Zr | 1449 | 1664 | 1395 | 1413 | 1218 | 1257 | 1114 | 1091 | 996 | 991 | 1175 |
| Nb | 310 | 375 | 308 | 342 | 284 | 326 | 265 | 266 | 259 | 252 | 278 |
| Th | 46 | 34 | 43 | 24 | 37 | 25 | 32 | 33 | 32 | 32 | 37 |
| U | 11 | 7 | 10 | 5 | 8 | 6 | 4 | 4 | 7 | 7 | 7 |
| Pb | 19 | 22 | 17 | 18 | 16 | 16 | 13 | 13 | 13 | 13 | 15 |
| Ga | — | 44 | — | 43 | — | 44 | — | — | — | — | — |
| Zn | 186 | 129 | 178 | 113 | 159 | 106 | 148 | 154 | 136 | 146 | 150 |
| Cu | b.d.l. | 4 | b.d.l. | 4 | b.d.l. | 4 | b.d.l. | b.d.l. | b.d.l. | b.d.l. | b.d.l. |
| Ni | 2 | 1 | 1 | 2 | 6 | 2 | b.d.l. | 1 | b.d.l. | b.d.l. | 1 |
| V | 36 | 38 | 35 | 40 | 35 | 42 | 15 | 18 | 29 | 17 | 37 |
| Cr | 9 | 3 | 9 | 3 | 9 | 3 | 5 | 1 | 6 | 6 | 5 |
| Hf | — | 25 | — | 21 | — | 19 | — | — | — | — | — |
| Cs | — | 3 | — | 3 | — | 2 | — | — | — | — | — |
| Sc | — | 13 | — | 13 | — | 12 | — | — | — | — | — |
| Ta | — | 14 | — | 15 | — | 16 | — | — | — | — | — |
| Co | 12 | 9 | 11 | 11 | 12 | 9 | 4 | 6 | 8 | 6 | 6 |
| Ge | — | 2 | — | 3 | — | 3 | — | — | — | — | — |
| La | 210 | 158 | 214 | 148 | 200 | 146 | 196 | 190 | 187 | 207 | 226 |
| Ce | 275 | 247 | 269 | 249 | 265 | 254 | 271 | 282 | 262 | 269 | 268 |
| Pr | — | 20 | — | 22 | — | 24 | — | — | — | — | — |
| Nd | 63 | 60 | 66 | 65 | 74 | 75 | 71 | 72 | 71 | 75 | 84 |
| Sm | — | 8 | — | 9 | — | 11 | — | — | — | — | — |
| Eu | — | 2 | — | 2 | — | 2 | — | — | — | — | — |
| Gd | — | 7 | — | 8 | — | 9 | — | — | — | — | — |
| Tb | — | 1 | — | 1 | — | 1 | — | — | — | — | — |
| Dy | — | 8 | — | 8 | — | 9 | — | — | — | — | — |
| Ho | — | 2 | — | 2 | — | 2 | — | — | — | — | — |
| Er | — | 6 | — | 5 | — | 6 | — | — | — | — | — |
| Tm | — | 1 | — | 1 | — | 1 | — | — | — | — | — |
| Yb | — | 6 | — | 5 | — | 5 | — | — | — | — | — |
| Lu | — | 1 | — | 1 | — | 1 | — | — | — | — | — |

Easting and northing coordinates are from zone 28 of the Universal Transverse Mercator grid for the northern hemisphere (WGS84 datum). Major elements have been normalized to 100 wt % volatile-free. Those samples with full trace element data have been analysed by ICP-MS, whereas samples with incomplete analyses by XRF and element abundances have been normalized on an anhydrous basis. b.d.l., below detection limit.

solutions (based on 1 : 50 dilutions of 50 mg, 100 mg and 150 mg of digested US Geological Survey rock standard BHVO-1) were prepared with each batch of samples. The STM-1 syenite standard was also used as a more appropriate standard with similar trace element and REE concentrations to Granadilla phonolite samples. Total dilution factors were calculated by weight for each sample and standard. US Geological Survey rock standards BHVO-1 and AGV-1 (and STM-1) served as check standards to monitor accuracy during analysis.

Diluted rock solutions were then analysed by ICP-MS using a VG PlasmaQuad PQ2+ in peak jumping mode with the electron multiplier operating in pulse-counting mode for maximum sensitivity and analytical precision. One or two isotopes were chosen for each element of interest based on considerations of isobaric interferences. Five blocks of data were obtained for each sample, with each block comprising 50 sweeps through the mass spectrum using three points per mass and five DAC steps per point. Instrumental drift corrections were accomplished using a combination of the In internal standard as well as repeat analyses of BHVO-1 (or STM-1 every five samples), permitting serial drift corrections on an element-by-element basis using an in-house data reduction computer program. Total analytical blanks (comprising both chemistry and mass spectrometer components) were typically <20 ppb for all elements, making blank corrections <2% for most geological samples and usually <0·1%. Precision (in-run statistics quoted as two standard errors of the mean) is typically better than 5% for each element. Determination of analytical accuracy has been based on multiple analyses of the US Geological Survey rock standards BHVO-1, AGV-1 and STM-1, and is typically better than 10% for most elements at the 95% confidence level. Exceptions include Gd, Dy and Er, which have light REE (LREE) oxide interferences, and Tb, Ho, Tm and Lu, which typically occur at very low concentrations.

### *Electron microprobe analysis*

Polished, and carbon-coated thin sections were analysed at the Centre for Microscopy & Microanalysis, University of Queensland, using a JEOL 8800-L (wavelength-dispersive) electron microprobe. Analyses were performed with an accelerating voltage of 15 kV and a probe current of 15 nA. Data were corrected on-line using the ZAF correction procedure. All phases were analysed with a 1 μm beam diameter, except for feldspars, biotite, kaersutite and glass, which were analysed using a beam diameter of 10 μm to avoid volatilization of alkali elements. During glass analyses, the stage was moved slowly and continuously to reduce the effects of alkali migration from the target volume (Neilsen & Sigurdsson, 1981). Precision and accuracy for each analytical run were checked by comparing results of a suite of geological and oxide standards of known composition, analysed at the start and end of each analytical run.

### *Oxygen isotope analysis*

Crystal and glass separates were prepared from lightly crushed pumice clasts using a tungsten carbide concentric ring mill. The crushed sample was sieved using 14 (1·4 mm diameter) and 100 (50 μm) mesh sieves. The >100 mesh fraction was used for mineral and glass separates, and washed to remove any fine glass, and dried. Minerals were separated from glass by heavy liquid methods. Feldspar, biotite, nosean and glass were then hand picked from the heavy liquid separates; composite grains or grains with inclusions were avoided.

Oxygen isotope ratios were measured at Monash University on a Finnigan MAT252 mass spectrometer. Oxygen isotope ratios of silicates were analysed following Clayton & Mayeda (1963) but using $ClF_3$ as the oxidizing reagent. The extracted gases were analysed as $CO_2$ and the results are expressed relative to V-SMOW. Internal and international standards run at the same time as the samples from this study generally yielded values within 0·2‰ of their accepted values. Long-term average $\delta^{18}O$ value of NBS 28 at Monash (as at 1998) is 9·55 ± 0·11‰.

## WHOLE-ROCK CHEMISTRY

### Major and minor elements

The chemistry of bulk-pumice and whole-rock ignimbrite samples of the Granadilla Member is plotted against stratigraphic height in Fig. 3. Stratigraphic variation in the major and trace element data can be grouped into the following: (1) those that show a continuous zonation lacking any step-like jumps in element abundances (e.g. $Fe_2O_3$, MnO, $P_2O_5$, Rb, Nb, Zr); and (2) those that show considerable scatter or inconsistent trends with stratigraphic height (e.g. $SiO_2$, alkalis, MgO, CaO). Although visibly fresh, some post-eruptive hydration of Granadilla pumices has occurred and is partly reflected by the relatively high LOI values (Table 2), and oxygen isotope compositions of pumice glass (see below). Carbonate cementation resulting from groundwater percolation is common within the Granadilla pumice, particularly along pumice fall bedding planes and the Unit 2–3 contact. Glass hydration and normalization of the major and trace element data on an anhydrous basis has partly contributed to the total variation in the concentration of major elements such as $SiO_2$ and $Al_2O_3$ in the dataset (see also Edgar *et al.*, 2002). However, little systematic variation in $SiO_2$ (~60·4–61·6 wt % anhydrous) is apparent up sequence. Increased scatter characterizes the more mobile elements CaO, MgO and the alkalis, where abundances in the Granadilla pumice have been

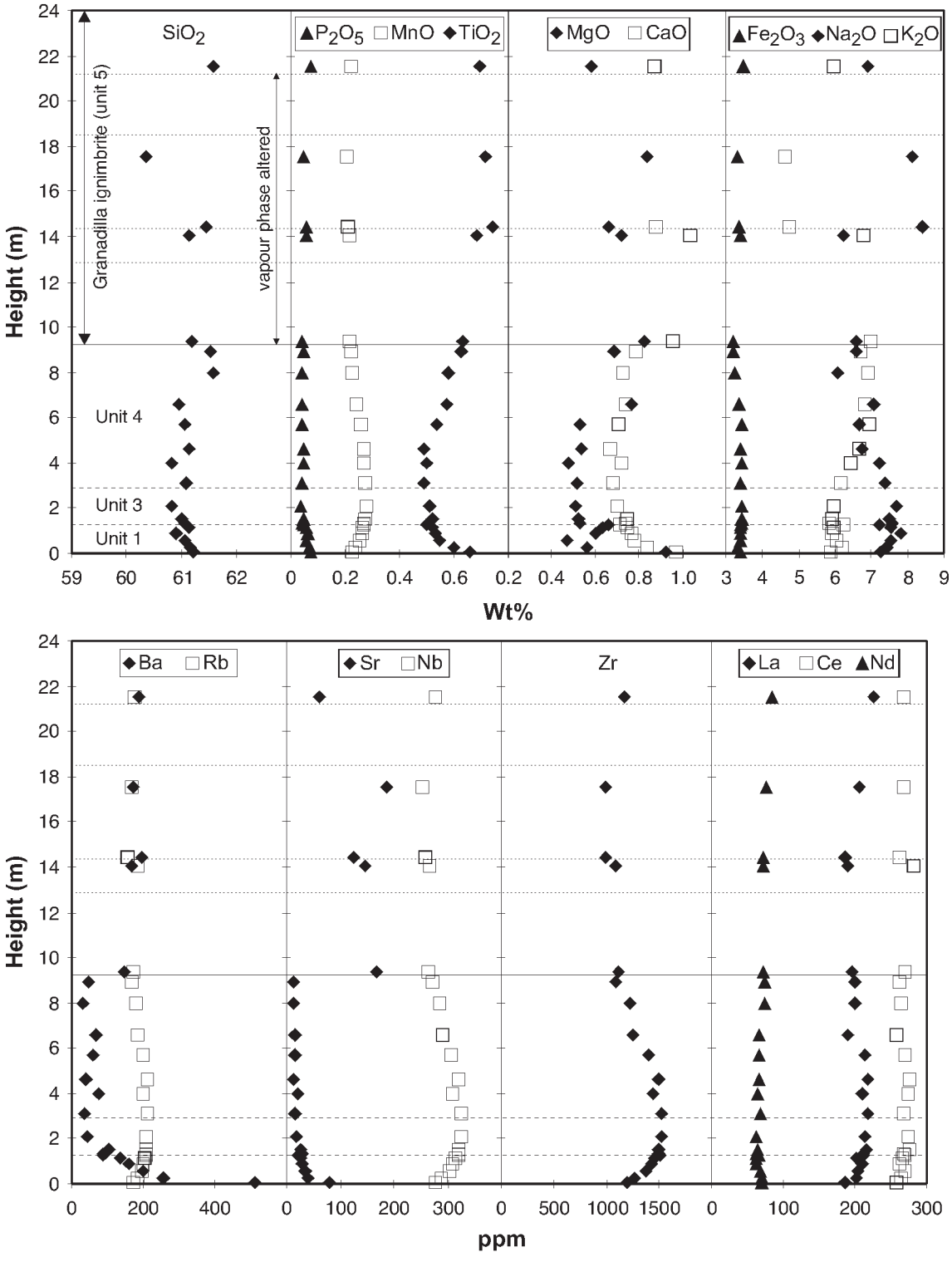


**Fig. 3.** Geochemical variation with stratigraphic height. The reverse-to-normal 'cryptic' compositional zonation of minor and trace elements at relatively constant $SiO_2$ should be noted (~61 wt %). Major and minor elements are normalized to 100% volatile-free, and trace elements are normalized on an anhydrous basis. However, increased scatter for the alkalis, MgO, CaO and Sr reflects element mobility, and is particularly prevalent in Unit 5 because of vapour-phase alteration. All data were obtained by XRF. Dashed lines are fall unit boundaries of the Granadilla pumice; dotted lines denote bedding in the Granadilla ignimbrite.

affected by post-eruptive, low-temperature exchange as a result of groundwater percolation. In addition, the alkalis, Sr, and CaO show considerable scatter within the vapour-phase altered Granadilla ignimbrite, whereas other more immobile elements (e.g. $Fe_2O_3$, MnO, $P_2O_5$, Ba, Nb, Zr) do not. The remainder of the discussion on bulk-pumice and ignimbrite chemistry is therefore focused on those elements whose abundances have not been affected by post-eruptive low-temperature alteration or vapour-phase alteration.

The immobile elements show slight but systematic and continuous variations up sequence, with two opposite trends (Fig. 3): a progressive increase from the base of Unit 1 to the base of Unit 4, followed by gradual decrease, for MnO and total iron as $Fe_2O_3$, whereas $TiO_2$ and $P_2O_5$ exhibit the reverse trend, being lowest in Unit 3 and at the base of Unit 4. Little compositional zonation is indicated from whole-rock samples of the Granadilla ignimbrite, which may reflect 'homogenization' processes during pyroclastic flow transport and deposition, where pumice and ash of different but potentially subtle composition have been abraded and mixed into the deposit (Bryan, 1998). Of the minor elements, $P_2O_5$ along with the more mobile MgO and CaO are distinctly higher in pumices from the base (Unit 1) compared with the top (Unit 4) of the Granadilla pumice (Fig. 3). Glass compositions of selected pumices analysed by electron microprobe generally exhibit the same vertical compositional trends as bulk-pumice samples (Fig. 4). However, the pumice glasses are notably more depleted in $TiO_2$, MgO, CaO and $K_2O$ compared with whole-pumice compositions, reflecting the absence of the observed phenocryst assemblage (Fe–Ti oxides, diopside, alkali feldspar and biotite). In comparison with pumice glasses from other Tenerife phonolite pyroclastic deposits, the Granadilla pumice glasses show some of the most extreme depletions in $TiO_2$ and $P_2O_5$ (as well as other elements), confirming that the eruption tapped a large volume of highly fractionated phonolitic magma (Bryan *et al.*, 2002).

### Trace elements

Trace element behaviour during evolution of the Tenerife phonolitic magmas can be differentiated into those elements behaving incompatibly (Rb, Th, Zr, Nb, Hf, LREE), those behaving compatibly (e.g. Sr, Sc), and those showing late-stage compatibility as a result of feldspar-dominated crystallization (Ba, Sr, Eu) or the appearance of titanite [e.g. Ta, middle REE (MREE); Wolff, 1984; see also Bryan *et al.*, 2002]. The vertical enrichment and depletion trends in the trace elements when plotted against deposit stratigraphy (Fig. 3) mirror those of the minor elements, and reflect this general behaviour. Vertical variations in the immobile trace element abundances typically show smooth, continuous trends, especially for the Granadilla pumice at approximately constant silica content [cryptic zonation of Bryan *et al.* (1998*a*), or occult zonation of Wolff & Storey (1984)]. The incompatible elements Rb, Zr, Nb and, to a lesser extent, Ce exhibit an upwards enrichment to Unit 3, followed by a gradual depletion through the main plinian fall Unit 4. All pumice compositions can be considered as high-Zr (>1000 ppm Zr; terminology of Edgar *et al.*, 2002) with the highest Zr contents in Unit 3 (1530 ppm by ICP-MS). The highest incompatible element abundances, therefore, characterize pumice from the central part of the deposit (Unit 3, base of Unit 4), indicating that the most evolved compositions were tapped during the main plinian phase of the eruption (Units 3 and 4). As noted by Wolff (1983), a reversal to more evolved compositions during the final stages of the eruption may be indicated by slight enrichments in Zr and Nb at the top of the ignimbrite (non-indurated facies), but the effects of particulate mixing and incorporation of pumices with higher incompatible element abundances via substrate erosion cannot be ruled out.

In an enrichment diagram (Fig. 5), comparing bulk-pumice compositions with the most evolved bulk-pumice composition from Unit 4 of the Granadilla pumice (as indicated by the highest incompatible element abundances), bulk-pumices from Unit 1 show very anomalous enrichments in Ba, Sr and Eu, as noted in previous studies (Wolff & Storey, 1984). The enrichment factor of Ba between pumice at the base (sample 111a) and Unit 4 pumices is the most significant (>10). In contrast, the comparison of bulk-pumice compositions from the middle and top of Unit 4 shows more systematic relative depletions in the incompatible elements such as Cs, Rb, Th, Pb, Zr and Hf. This is consistent with bulk-pumice compositions from the top of Unit 4 representing less fractionated magma compositions (Fig. 3), as previously suggested by Wolff (1983).

## PUMICE PHENOCRYST CHEMISTRY

Granadilla pumices contain the phenocryst assemblage alkali feldspar + biotite + titanite + nosean/haüyne + sodian diopside + titanomagnetite + ilmenite + apatite, with alkali feldspar being the dominant phenocryst phase in all units (Table 1). Kaersutite and plagioclase are subordinate phenocryst phases in pumices from Units 1 and 3, and in the upper parts of the Granadilla ignimbrite (Unit 5). Kaersutite also occurs as crystal grains in Units 2 and 5. Blebs of crystal-rich, weakly vesicular glass are relatively common in pumices from Unit 1 and contain fine-grained intergrowths of plagioclase, kaersutite, Fe–Ti oxides ± apatite (Fig. 6a). Overall, Granadilla pumices are crystal-poor (Table 1).

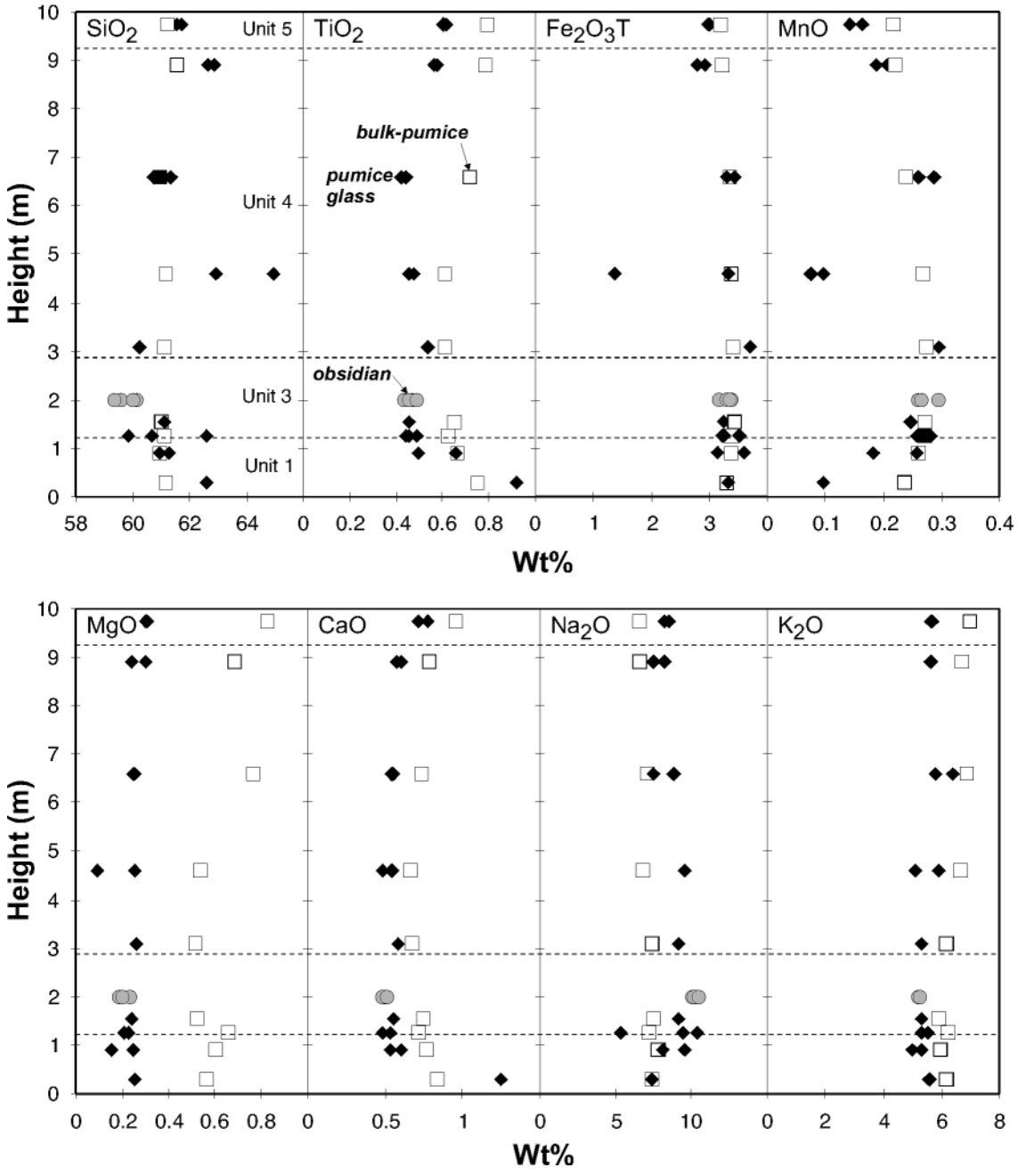


**Fig. 4.** Major element chemistry of pumice glass (filled symbols), juvenile obsidian clasts (grey symbols) and bulk-pumice (open symbols) vs stratigraphic height. Glass compositions were determined by electron microprobe and normalized to 100 wt % (see Bryan *et al.*, 2002). Bulk-pumice data have been normalized to 100 wt % volatile-free. Dashed lines are fall unit boundaries of the Granadilla pumice. The anomalous glass chemistry ($TiO_2$, CaO, MnO) at the base should be noted.

## Feldspar

Tabular, subhedral to euhedral feldspar phenocrysts (1–3 mm long) are characteristic. Some resorption of feldspars is shown by rounded corners and occasionally embayed phenocrysts (Fig. 6b). Typical inclusions in feldspar are biotite and to a lesser extent, nosean/haüyne.

Feldspar phenocryst compositions are illustrated in Fig. 7. Up sequence, phenocryst compositions in most samples show a relatively restricted range from potassic anorthoclase to sodic sanidine ($Or_{30–40}$). In some pumices, however, two or three compositionally distinct feldspar populations occur, with the presence of plagioclase (calcic anorthoclase to andesine) in addition

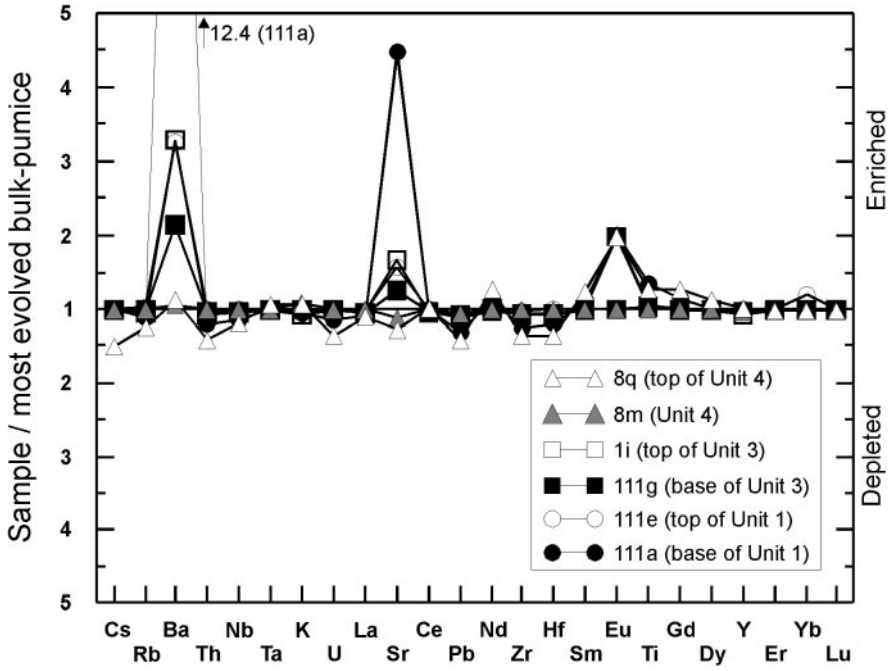


**Fig. 5.** Enrichment diagram (Hildreth, 1979) for the Granadilla pumice. Element concentrations for each sample have been divided by the concentration of the same element in sample 8k, the most evolved bulk-pumice composition (Table 2). The anomalous to extreme enrichment in Ba (12·4 times), Sr and Eu of bulk-pumice compositions from the base should be noted. Bulk-pumice compositions from the top of the Granadilla pumice, represented by sample 8q, show more systematic relative depletions in the incompatible elements (e.g. Cs, Rb, Th, Zr, Hf).

to K-feldspar (Fig. 7). Plagioclase is resorbed (Fig. 6b), whereas the dominant sodic sanidine–potassic anorthoclase phenocryst population shows no evidence of resorption. Calcic anorthoclase and oligoclase to sodic andesine plagioclase feldspars are characteristic of tephriphonolite magma compositions (see Bryan *et al.*, 2002). Plagioclase feldspars are most prevalent in pumice sampled from the base of fall units (e.g. base of subunit 1b—sample 111b; base Unit 3—sample 111g; base Unit 4—sample 8k; Figs 2 and 7), which are typically coarser grained than the preceding fall unit, or from coarser pumice beds within fallout units (e.g. Unit 3—sample 1i; Fig. 7). Feldspar compositions from pumice clasts within the Granadilla ignimbrite overlap in composition with crystal grains supported in the vitric ash matrix, although the feldspar grains often show a wider range of compositions (e.g. sample 6t, Fig. 7).

Feldspar phenocryst core to rim relationships (Fig. 8) reveal: (1) generally weak zoning ($\leq$5% Or) in the alkali feldspars; (2) the presence of both normally and reversely zoned phenocryst populations in many samples; (3) an absence of strong zoning in feldspar grains from the phreatoplinian Unit 2; and (4) either unzoned or strongly normally zoned plagioclase and calcic anorthoclase phenocrysts (e.g. samples 111a, 111g and 6t of Fig. 8). The strong normal zoning of the calcic anorthoclase crystal population is consistent with the transfer of these phenocrysts into more evolved magma compositions, whereas reverse zoning of sanidine records crystallization in the presence of less evolved magma.

Important minor element substitutions in the feldspars include Fe and Ba. Barium is a distinctive minor element, with some feldspars containing up to 2 wt % BaO (Fig. 9). Although Ba replaces K within the feldspar structure, the most potassic sanidines have the lowest contents of Ba. Calcic anorthoclase phenocrysts ($Or_{10–20}$) contain the highest abundance of Ba (Fig. 9) and Ba contents decrease sharply with increasing Or content above $Or_{20}$ (see also Bryan *et al.*, 2002). Ba-rich feldspars are particularly abundant in pumices of Unit 1.

## Clinopyroxene

Sodic clinopyroxene ($\leq$1 mm diameter) typically occurs in small glomerocrysts with titanomagnetite and titanite. All clinopyroxene phenocrysts are characteristically light green, weakly pleochroic, and occur as euhedral, prismatic crystals. Twinning is occasionally observed.

Microphenocrysts are mainly sodian diopside [following the terminology of Morimoto *et al.* (1988)] in composition ($En_{39}Fs_{15}Wo_{46}$ to $En_{27}Fs_{30}Wo_{43}$), and show a systematic decrease in Wo content with increasing Fe, and define a continuous solid solution series to aegirine–augite compositions (Fig. 10). Clinopyroxenes from other Tenerife phonolites plotting close to the diopside–hedenbergite join were designated as salites in early

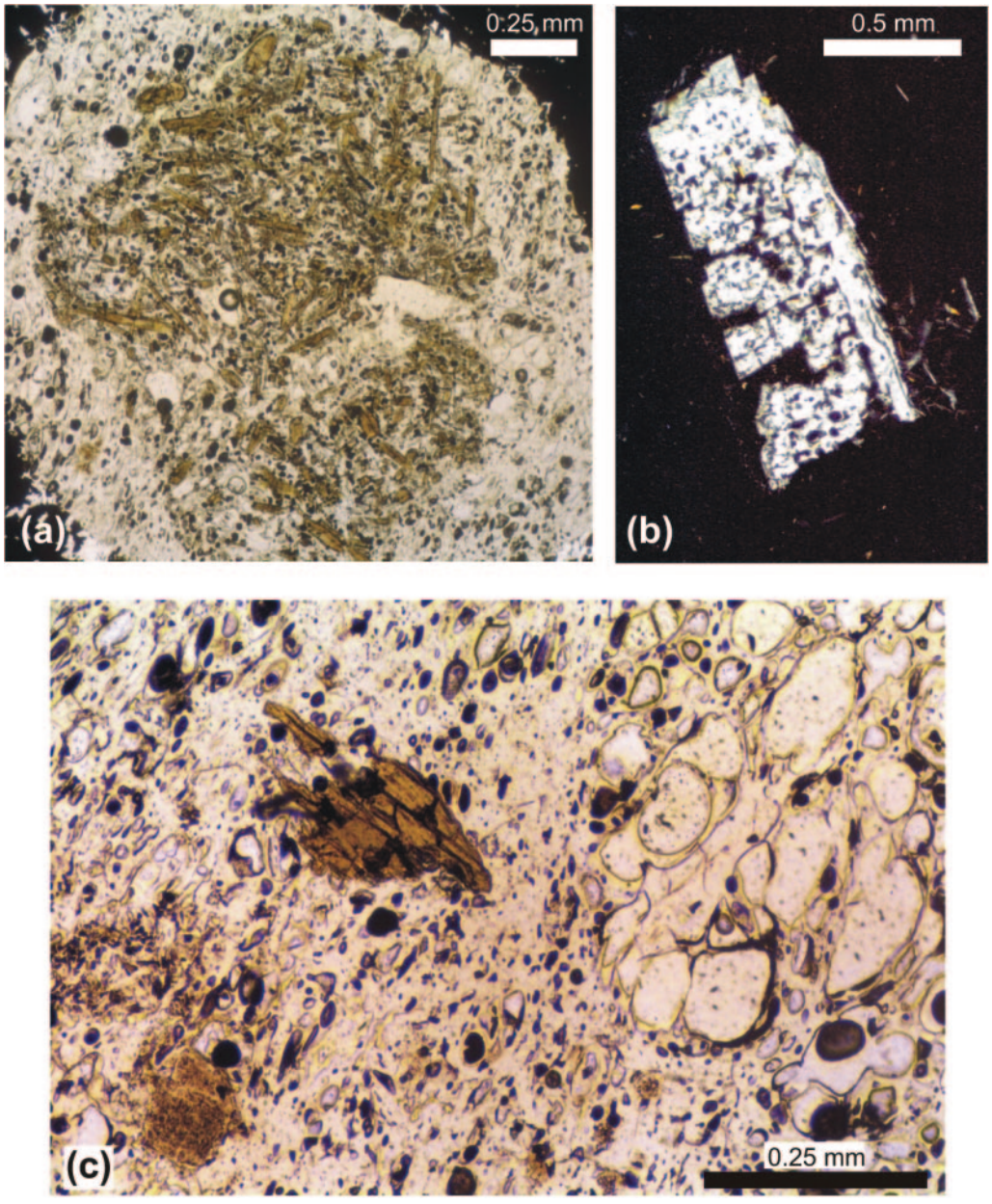


**Fig. 6.** Photomicrographs of pumice textures. (a) Tephriphonolitic glass bleb comprising fine-grained intergrowths of kaersutite, plagioclase, Fe–Ti oxides ± apatite (sample 111g). Width of view is 1·7 mm; plane-polarized light. (b) Resorbed calcic anorthoclase ($An_{12}Ab_{69}Or_{19}$) phenocryst in pumice clast from subunit 1B (sample 111b). Length of phenocryst is 1·5 mm; crossed polars. (c) Banded pumice from Unit 3 (sample 111g) preserving the mingling of poorly vesiculated (containing kaersutite) and highly vesiculated glass domains. Width of view is 1 mm; plane-polarized light.

studies (e.g. Scott, 1976). Phenocrysts from Unit 4 pumices (samples 8k, 8o, 8q of Fig. 10) exhibit the least variation, and include some of the more Fe-rich compositions. Samples with a wider scatter of pyroxene compositions (e.g. 111g, 1i and 6t) correspond to those with bimodal feldspar compositions (Fig. 7). Ti–Al relationships for clinopyroxene show a wide variation in Al in the tetrahedral site relative to Ti. Pyroxenes conform closely to a ratio of 1 : 2, but show an excess of $Al^{IV}$ over Ti, which is a feature observed in other volcanic rocks from Tenerife and has been related to the solid-solution of the Ca-Tschermak's component ($CaAlAlSiO_6$, Scott, 1976; Wolff, 1983).

In contrast to the feldspars, most clinopyroxene phenocrysts are unzoned but a small population of phenocrysts, predominantly in the Granadilla ignimbrite (Fig. 10), exhibit reverse zoning in terms of aegirine content (up to 10% Ae; Bryan, 1998).

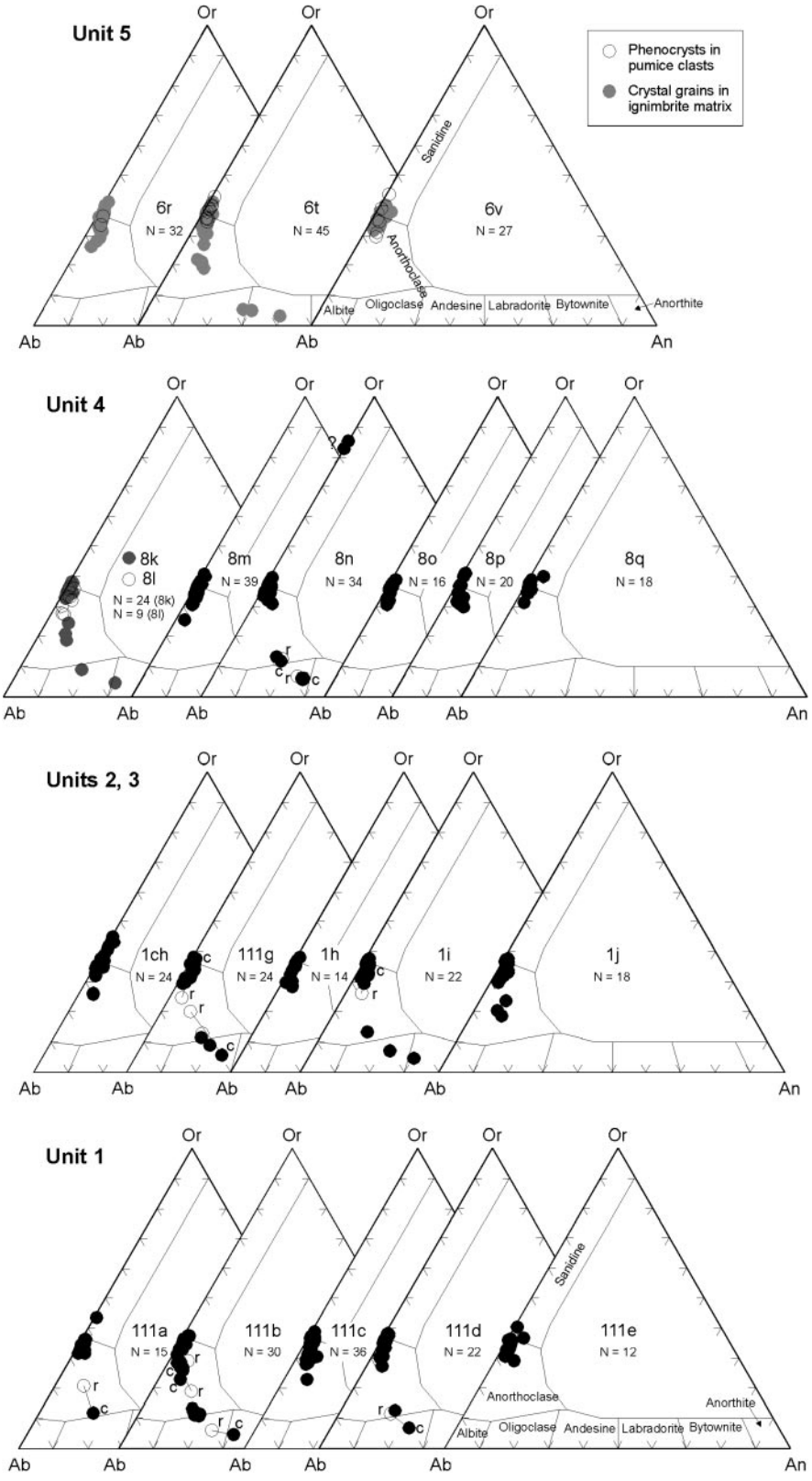


**Fig. 7.** Albite (Ab)–anorthite (An)–orthoclase (Or) triangular diagrams showing feldspar compositions from the Granadilla pumice and ignimbrite. N, number of analyses. Selected core (c) and rim (r) pairs with tie-lines are shown for samples 111a, 111b, 111d, 111g, 1i and 8n.

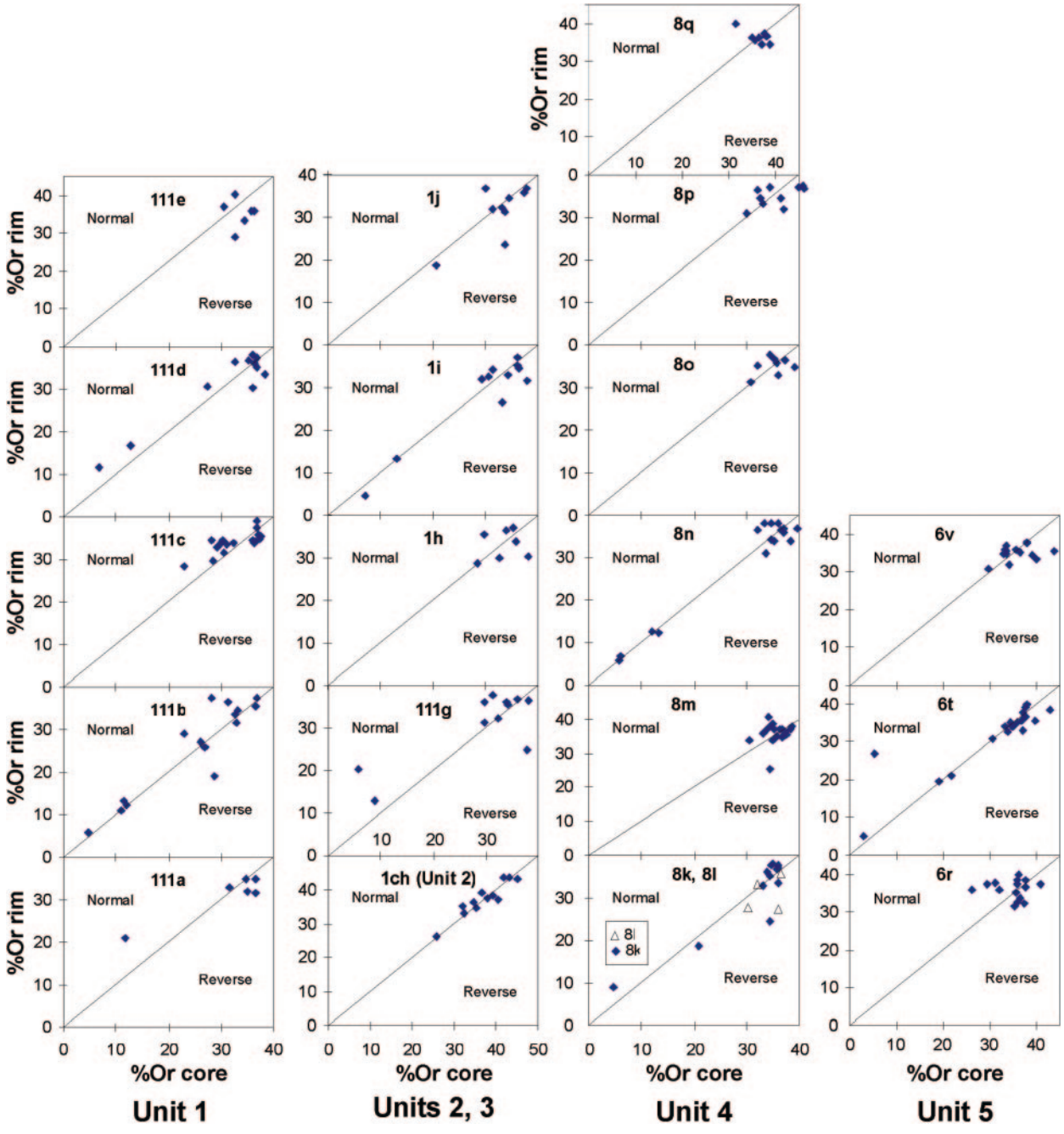


**Fig. 8.** Zoning patterns of feldspar phenocrysts for individual samples, based on orthoclase (Or) content (molecular per cent), and arranged in stratigraphic order for each unit. Core and rim analyses are plotted to illustrate the growth history of individual phenocrysts. Feldspar phenocrysts will tend towards higher orthoclase contents during fractional crystallization of phonolite magma under closed-system conditions, resulting in normal compositional zoning. Reverse compositional zoning indicates disturbance of the system (e.g. the introduction of mafic magma). Normal and reversely zoned feldspar phenocrysts are present in most samples. In contrast, a small population of unzoned plagioclase phenocrysts is present in samples 111b, 1i, 8n and 6t, suggesting that these plagioclase phenocrysts were mingled into the magma either immediately prior to or during the eruption.

## Biotite

Biotite is the main ferromagnesian phase in the Granadilla pumices. Phenocrysts ($\leq$2 mm long) are typically euhedral, and commonly contain inclusions of apatite and, to a lesser extent, titanomagnetite. Biotite is occasionally, partly or completely enclosed by feldspar. Biotite compositions are remarkably uniform up sequence. They are Mg-rich (Mg/(Mg + Fe) $\sim$0·6–0·55),

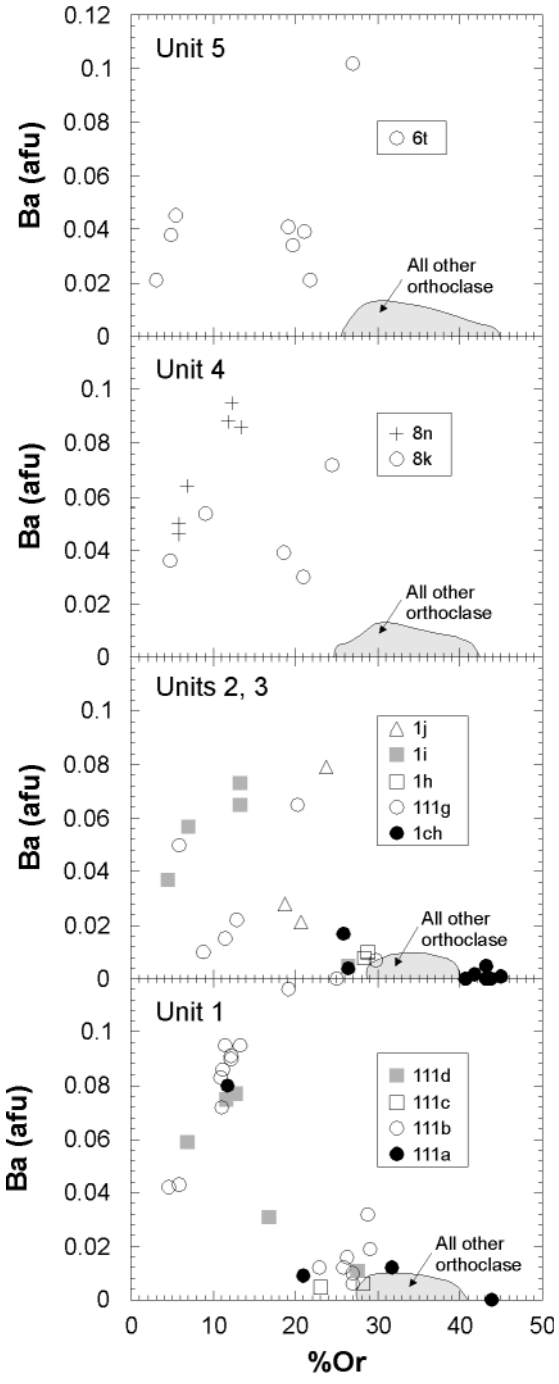


**Fig. 9.** Ba (atoms per formula unit) vs Or (molecular per cent) content of feldspar phenocrysts. The dominant orthoclase feldspar phenocrysts have very low Ba abundances (<0·01 a.f.u.), whereas the highest abundances occur in the calcic anorthoclase phenocrysts.

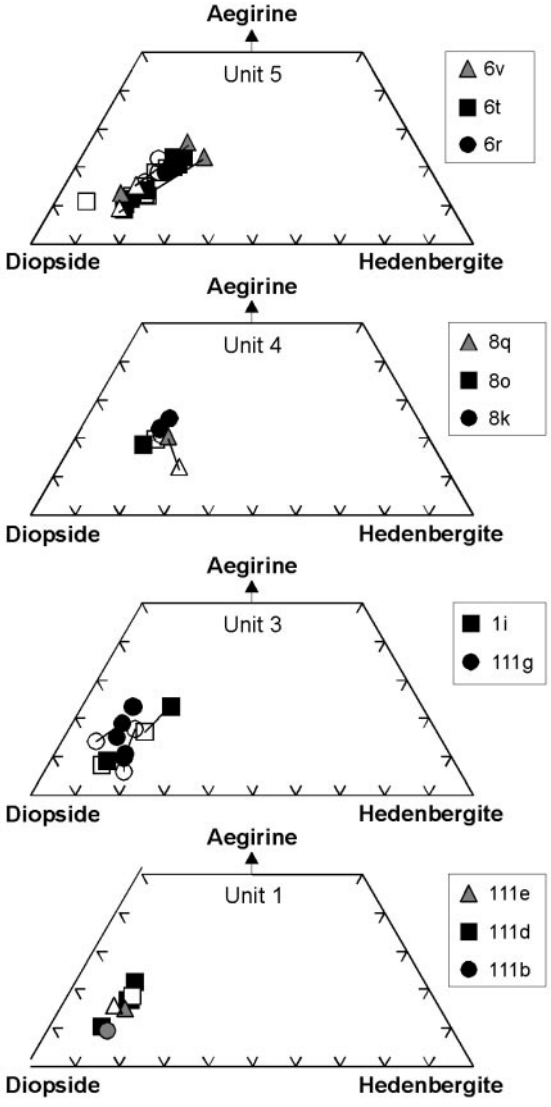


**Fig. 10.** Pyroxene microphenocryst compositions expressed in terms of the diopside, hedenbergite and aegirine end-members. Filled symbols represent core compositions; open symbols, rim compositions. Tie-lines are shown for selected phenocrysts, and generally strong reverse zoning patterns (up to 10% aegirine) occur in pyroxenes with sodic-rich cores (Unit 5).

with the most Fe-rich biotites occurring towards the middle of the sequence (top of Unit 3). Most biotites have less Al than necessary to fill the tetrahedral site, a common characteristic of biotites in alkaline rocks (e.g. Jones, 1984; Schneiderman, 1991; Loferski & Ayuso, 1991). Na is high (>0·12 a.f.u.) and the sum of cations in the X site (Ca + Na + K + Ba) is ~1. Rb has been detected only at trace levels in the biotites, and Ba, although variable (up to 1·2 wt % BaO), is the most important minor element substitution in the X site. Biotites are characteristically Cl-poor (mostly <0·3 wt %) and show a significant range in F content (0·25 – 0·92 wt %), with most in the range 0·6–0·9 wt % F. The restricted composition of biotite suggests that the variation in F and Cl contents is not due to Fe–F avoidance (Munoz, 1984), but

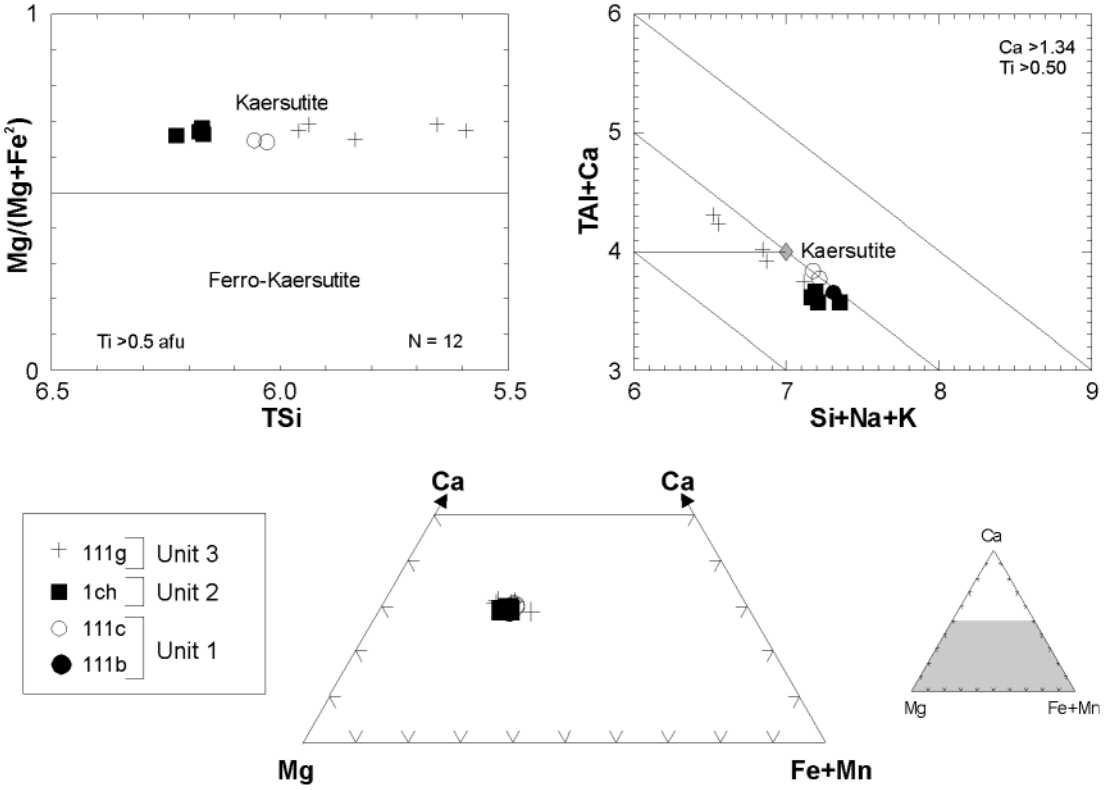


**Fig. 11.** Phenocryst amphibole compositions. Cation proportions are based on the 13 − (Ca + Na+ K) normalization procedure. The prefix T denotes cation in the tetrahedral site. N, number of analyses.

may be dependent on temperature and on the relative fugacities of the halogens during crystallization.

## Kaersutite

Rare phenocrysts of kaersutite (Fig. 6c) are present within the pumices of Unit 1, at the base of Unit 3, and Unit 5, and as crystal grains in the phreatoplinian Unit 2. Kaersutite in pumices from Units 1 and 3 is associated with small blebs of darker, poorly vesicular glass containing fine-grained feldspars, Fe–Ti oxides and kaersutite (Fig. 6a). Bands of less vesicular glass containing kaersutite microphenocrysts characterize some pumices at the base of Unit 3 (Fig. 6c). Kaersutite shows no disequilibrium textures, and is generally euhedral in form, in contrast to that observed in the phonotephritic lavas of Tenerife, which is rimmed or almost wholly replaced by Fe–Ti oxides (Bryan, 1998).

Kaersutites are poor in Si (<6·3 a.f.u.; Fig. 11), although no Ti is required in the tetrahedral site. Ca contents (≥1·8 a.f.u.) indicate almost total occupancy of the B site by Ca; there is little variation between samples in terms of Ca–Mg–Fe contents (Fig. 11). Fluorine contents are variable but mostly low (<0·2 a.f.u.), indicating only minor replacement in the hydroxyl site. Cl is mostly below detection limit.

## Fe–Ti oxides

Small Fe–Ti oxide grains typically occur in glomerocrysts with pyroxene and/or titanite. Apatite is a common inclusion within titanomagnetite. Titanomagnetite is occasionally enclosed by biotite and, rarely, feldspar phenocrysts. Both titanomagnetite and ilmenite are also found as microphenocrysts, although ilmenite is always subordinate to titanomagnetite. Ilmenite has not been observed to be included by other phases, and is interpreted to have precipitated late in the crystallization sequence.

Ulvöspinel solid-solution [estimated following the method of Carmichael (1967)] in the titanomagnetites ranges from $Usp_{27}$ to $Usp_{43}$, whereas ilmenite shows a restricted compositional range ($Ilm_{88–93}$). The highest ulvöspinel contents are found in titanomagnetites from subunit 1b. Titanomagnetites from Unit 5 are characterized by higher ulvöspinel contents than in the preceding pumice fallout (Unit 4). Titanomagnetites are essentially unzoned, in contrast to the more complex zoning relationships of feldspar in the same samples.

The Fe–Ti oxides are enriched in minor elements, consistent with their growth from silica-undersaturated melts (Carmichael *et al.*, 1970). A spread of titanomagnetite compositions, based on minor element chemistry,

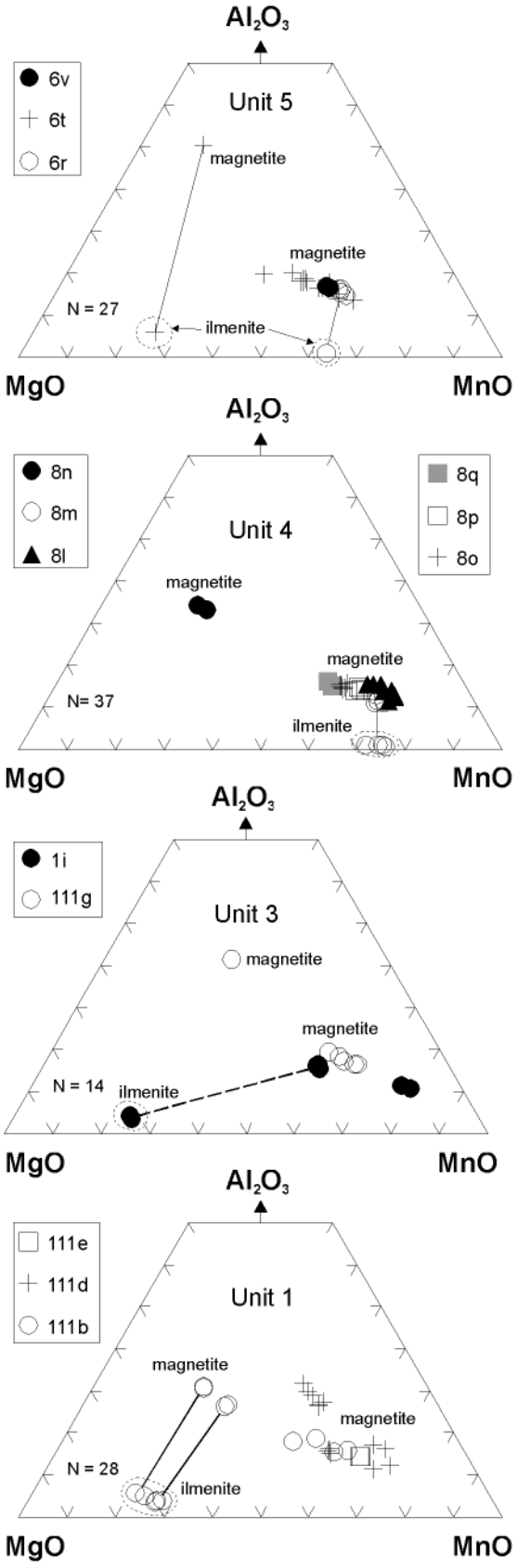


is observed (Fig. 12), although most are Mn-rich (up to 4 wt % MnO). The major changes within the sequence are the MnO enrichment and MgO depletion in both the spinel and ilmenite phases (Fig. 12). MgO and $Al_2O_3$ contents are lowest in titanomagnetite in pumice from the middle of the sequence (sample 1i, top of Unit 3; samples 8l and 8m, base of Unit 4). Of significance is the presence of several compositionally distinct Fe–Ti oxide phases within the same pumice sample (e.g. samples 111b, 111d, 111g, 1i and 6t of Fig. 12), mainly within the basal fallout and top ignimbrite units. For some samples (e.g. sample 1i of Fig. 12), these would give discordant tie-lines between coexisting Fe–Ti oxide minerals, indicating disequilibrium between these coexisting compositions (Carmichael, 1967).

## Nosean/haüyne

Microphenocrysts of nosean or haüyne (≤2 mm diameter) are distinctive within pumices because of their bright, azure blue colour, and euhedral (cubic) form. They vary in colour from blue to white and grey, with colour banding (zoning) observed in some phenocrysts.

In terms of Na–Ca–K components (Fig. 13a), the feldspathoid is low in K and shows a range of Ca contents (≤8 wt % CaO), which defines a gradation in composition from sodalite to haüyne. Most microphenocrysts, however, plot within the nosean field of Lessing & Grout (1971), and are distinguished from true sodalite by their high sulphur contents (up to 11 wt % $SO_3$). A more sodic-rich nosean occurs in pumices from the central parts of the Granadilla pumice (top of Unit 3, base of Unit 4) that is characterized by higher Cl contents (Fig. 13b). Core–rim analyses reveal some chemical zoning with increasing $SO_3$, K ± Ca towards phenocryst rims. The presence of nosean/haüyne requires that sulphur existed within the melt (or as a separate fluid phase) mostly as the oxidized species, which may indicate unusually high $fO_2$. Stormer & Carmichael (1971), however, considered that the occurrence of sulphate rather than sulphide is controlled more by the silica activity of the magma, as exemplified by the following reaction:

$$\underset{\text{nosean}}{Na_8Al_6Si_6O_{24}(SO_4)} + \underset{\text{magnetite}}{Fe_3O_4} + 16SiO_2 = \underset{\text{liquid pyrrhotite}}{FeS} + \underset{\text{aegirine}}{2NaFeSi_2O_6} + \underset{\text{albite}}{6NaAlSi_3O_8} + \underset{\text{gas}}{2O_2}.$$

Falling silica activity will drive the reaction to the left. Pyrrhotite is present in Tenerife mafic rocks

**Fig. 12.** Minor element chemistry of titanomagnetite and ilmenite (circled). Tie-lines (continuous lines) join coexisting phases in equilibrium, whereas the discordant tie-line (dashed line) for sample 1i of Unit 3 illustrates disequilibrium between the coexisting Fe–Ti oxide compositions. N, number of analyses.

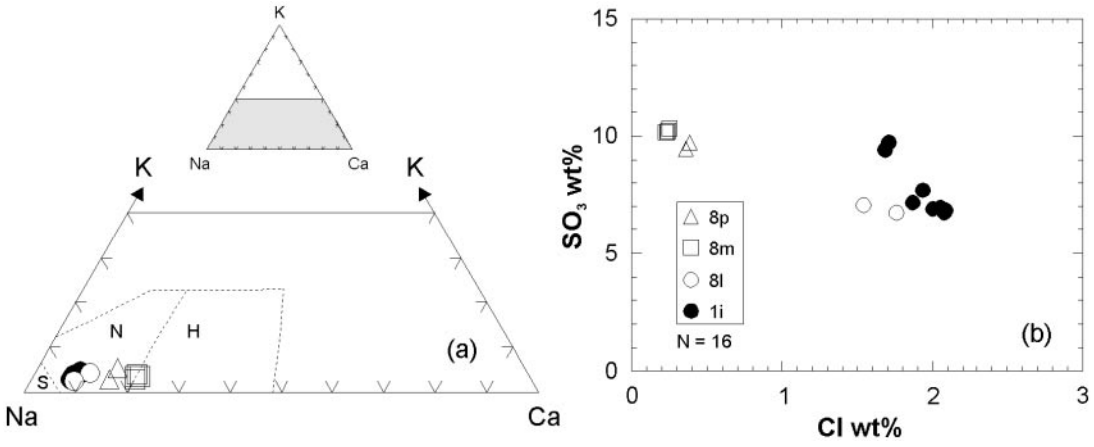


**Fig. 13.** Nosean phenocryst compositions expressed in terms of (a) Na, K, and Ca (atomic per cent), and (b) $SO_3$ vs Cl content (N, number of analyses). Field boundaries in (a) are after Lessing & Grout (1971). S, sodalite; N, nosean; H, haüyne.

(e.g. Wolff & Storey, 1983), but as the magmas evolve to phonolitic compositions, $SiO_2$ and/or $Al_2O_3$ activities decrease in response to a combination of kaersutite fractionation from tephriphonolite to phonolite, followed by the fractionation of alkali feldspar + biotite in the phonolite magmas (see Ablay *et al.*, 1998). Consequently, the above reaction is driven to the left and nosean forms part of the crystallizing assemblage in the Tenerife phonolites.

### Titanite

Golden yellow, euhedral phenocrysts and microphenocrysts of titanite are present within pumices and ignimbrite of the Granadilla Member, commonly occurring in small glomerocrysts with titanomagnetite and sodian diopside. Titanite analyses show variable, but high, Zr contents (up to 2·4 wt % $ZrO_2$), ~1 wt % $Nb_2O_5$ (Fig. 14) and moderate LREE (La, Ce) abundances (0·5–1 wt %). Fluorine contents (up to 0·5 wt %) are higher than Cl (trace levels only). Octahedral sites are Ti deficient (~0·9 a.f.u.), requiring some $Fe^{III}$, Al and/or Zr substitution (Higgins & Ribbe, 1976). Although the association of titanite and titanomagnetite is thought to reflect relatively high $fO_2$ (Lipman, 1971), in alkaline magmas the presence of titanite is stabilized by the low silica activity (Wolff, 1983, 1984).

### Apatite

Apatite typically occurs as inclusions within titanomagnetite and biotite phenocrysts, but also as inclusions within sodian diopside and K-feldspar. The apatites are fluorapatites [F/(F + Cl + OH) > 0·5], containing high amounts of LREE (up to 8 wt %), with $Ce_2O_3$ predominant over $La_2O_3$, $SiO_2$ (up to 3·5 wt %), and $SO_3$ (up to 0·7 wt %). There is no observable relationship between apatite chemistry and stratigraphic height, with most samples exhibiting a range of $SO_3$, $SiO_2$ and LREE contents (Fig. 15). Sample 8n (middle of Unit 4) is notable for containing the highest analysed $SO_3$ contents. The anomalous $SiO_2$ contents are real, as many high-Si apatites occur as inclusions within titanomagnetite. The uniformly low Cl content (≤0·2 wt %; Fig. 15c), and the consistently low Cl contents of the other hydrous phenocryst phases (biotite, kaersutite, nosean) suggest an overall low $P_{Cl}$ or greater incompatibility of Cl in the crystallizing phases.

## INTENSIVE PARAMETERS

### Temperature and $fO_2$

Estimates of temperature and $fO_2$ for the Granadilla pumice are based on the compositions of coexisting Fe–Ti oxides (Fig. 16a), using core–core and rim–rim mineral pairs in the same sample, and the recalculation program and procedures of Ghiorso & Sack (1991). Titanomagnetite–ilmenite pairs were checked for Mg/Mn equilibrium (Bacon & Hirschmann, 1988; Fig. 16b), and those with clearly discordant tie-lines (e.g. sample 1i of Fig. 12) were rejected from the calculations. The Fe–Ti oxide temperature estimates are thought to approximate those when the titanomagnetite–ilmenite–liquid equilibrium was quenched by the eruption. A range of temperatures from ~800 °C to 990 °C is given by the coexisting Fe–Ti oxides (Fig. 16a). There is a stratigraphic variation in temperature (Fig. 16c), which initially decreases up sequence from ~944 °C (Unit 1), 864 °C (core pairs) to 804 °C (rim pairs) in Unit 4, to a minimum of 793 °C at the base of Unit 5, and followed by an increase to >900 °C towards the top of Unit 5. The lowest temperature magmas were erupted during the main plinian phase of the eruption (Unit 4 to base of Unit 5). Oxygen fugacity estimates plot ~0·5 log units

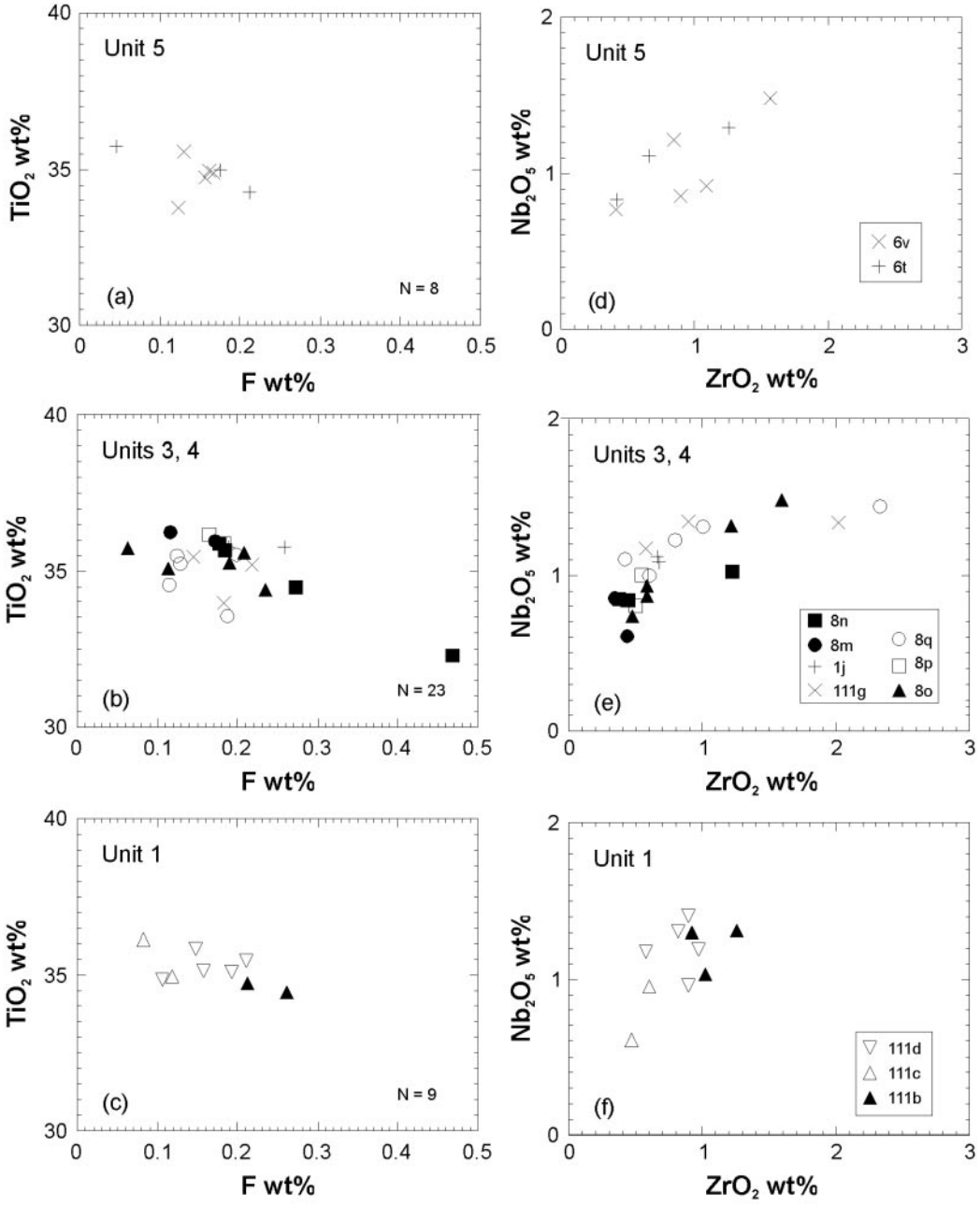


**Fig. 14.** Titanite chemistry expressed in terms of $TiO_2$ vs F content (a–c) and $Nb_2O_5$ vs $ZrO_2$ (d–f). N, number of analyses. The highest Zr contents are observed in titanites from pumices from the main plinian fall units (Units 3 and 4).

above the NNO (nickel–nickel oxide) buffer (see Ablay *et al.*, 1998), but define a $T$–$fO_2$ trend that approaches the NNO buffer at low temperatures (Fig. 16a).

Application of the biotite geothermometer of Luhr *et al.* (1984), based on the coupled exchange of Ti and $Fe^{2+}$, yields a greater range (~760–1370 °C) and, generally, higher temperature estimates than calculated from the Fe–Ti oxide data (see Fig. 17). This variability is probably partly due to the difficulties in determining $Fe^{3+}$ and $Fe^{2+}$, which are estimated from charge balance considerations, as well the effect of octahedral vacancies produced by Ti substitution. Calculations using octahedral Ti only, yielded temperature estimates of 800–900 °C that compare more favourably with the Fe–Ti oxide geothermometry. These data show a similar temperature trend to the Fe–Ti oxide data with higher temperatures at the base, and minimum eruptive temperatures for the main plinian phase of the eruption (Units 3–5; Fig. 17).

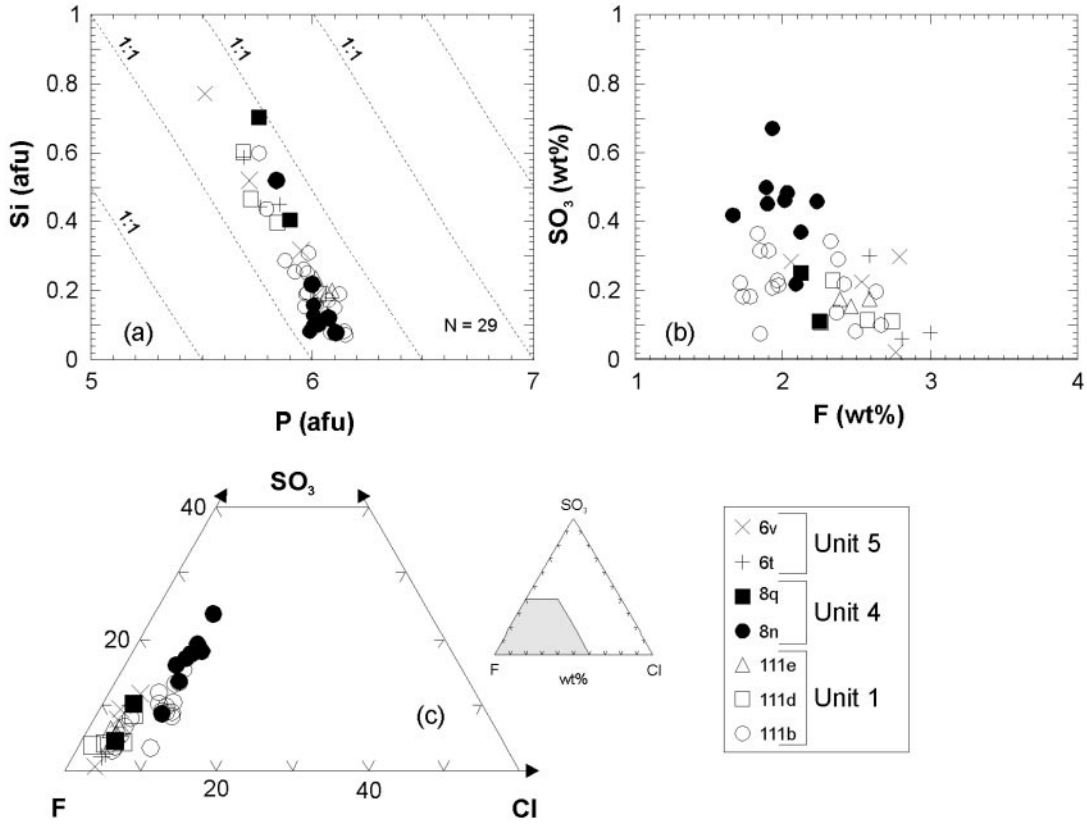


**Fig. 15.** (a) Si vs P (O = 26); (b) $SO_3$ vs F; (c) $SO_3$–F–Cl relationships for apatite microphenocrysts and inclusions. N, number of analyses. As with the coexisting nosean phenocrysts, the highest $SO_3$ contents occur in apatites from Unit 4.

In summary, the stratigraphic variation in calculated temperatures suggests a thermal gradient through the magma chamber. Higher equilibration temperatures for Unit 1 indicate that the eruption commenced with relatively hot phonolitic magma, with the higher temperatures probably in response to magma mixing or mingling with hotter (>940 °C), more mafic magma as indicated by petrographic and mineral chemical data (Figs 6a, 8 and 12). Fe–Ti oxide and biotite thermometry indicates that the main plinian phase of the eruption (Units 3 and 4, and the base of Unit 5) was characterized by eruption of magma with the lowest eruptive temperatures, whereas higher temperature magma was tapped during the latter stages of the eruption and emplacement of the upper parts of Unit 5 (Granadilla ignimbrite; Fig. 16).

## Water fugacity

If temperature and the oxygen fugacity are independently known, the water fugacity can be calculated from the assemblage of sanidine + biotite + magnetite (Wones, 1972). Water fugacity calculations (Table 3) show a distinct gradient in water fugacity values, deceasing upwards from Unit 3 to 5. The low water fugacity value estimated from the Granadilla ignimbrite (sample 6r, Table 3) suggests that tapping of less gas-rich levels of the chamber may have contributed to column collapse, producing pyroclastic flows. The main plinian phase of the eruption is, however, characterized by the highest water fugacity estimates. This is confirmed by bulk-pumice vesicularity measurements (Table 1) indicating that pumices from Unit 3 have the highest vesicularities and that a general decrease in clast vesicularity occurs upwards through Unit 4 (Fig. 2).

## Stable isotope chemistry

### *Oxygen*

O isotope analyses of glass, feldspar and biotite mineral separates for a representative set of Granadilla samples are given in Table 4. $\delta^{18}O$ values for the feldspar separates range from +6·3 to +7·1‰, and for biotites from +4·8 to +6·4‰, consistent with typical magmatic values (see Taylor, 1968). Limited data for basalts from the Canary Islands give $\delta^{18}O$ values of +5·4 to +5·9‰ (Harmon & Hoefs, 1995), which may be considered

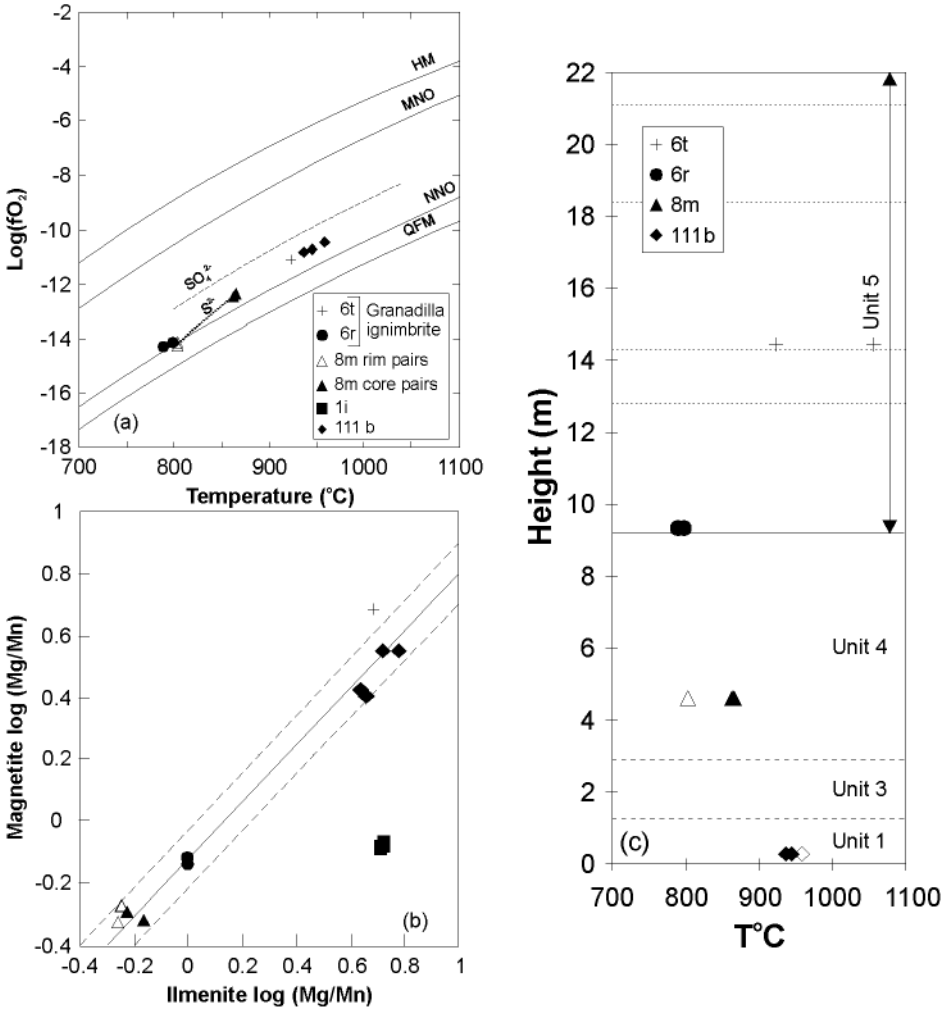


**Fig. 16.** (a) Temperature and oxygen fugacity ($fO_2$) estimates obtained from coexisting Fe–Ti oxides. Buffer curves are from Rutherford (1993): HM, hematite–magnetite; MNO, MnO–$Mn_3O_4$; NNO, Ni–NiO; QFM, quartz–fayalite–magnetite. Dotted line joins core and rim pairs of sample 8 m. (b) Mg/Mn (atomic) ratio of oxide pairs used in geothermometry calculations compared with the equilibrium field of Bacon & Hirschmann (1988), with dashed lines being a $2\sigma$ error envelope. It should be noted that the Fe–Ti oxide pairs from sample 1i (Unit 3) are not in equilibrium, as evidenced by the discordant tie-line slope in Fig. 12. Symbols are as for (a). (c) Fe–Ti oxide temperature estimates vs stratigraphic height. Filled symbols represent core pairs; open symbols, rim pairs.

representative of the primary magma. Oxygen isotope compositions of glass separates are distinctly higher in $\delta^{18}O$, ranging from +12·9 to +15·0‰ (Fig. 18). Distinct shifts in the glass O isotopic composition are observed at the contact between Units 2 and 3, and to a lesser extent, across the contact of Units 3 and 4 (Fig. 18). The isotopically heavier O values for pumice glass come from samples collected at four localities (Fig. 1). Consequently, the isotopic compositions are interpreted to be representative of pumice glasses for the Granadilla Member.

*Sulphur*

$\delta^{34}S$ values for four nosean crystal separates, one each from Units 1 and 3, and two from the main plinian fall Unit 4 were published by Bryan *et al.* (2002), and show a relatively restricted range from +6·1 to +8·8‰ (Fig. 18). The sulphate is distinctly heavier than sulphide gases analysed from active fumaroles on Teide (–0·6 to −1·3‰), but compares well with sulphate emissions (+4·5 to +6‰) in underground water tunnels across Tenerife (Albert-Beltran *et al.*, 1990; Valentin *et al.*, 1990). The nosean sulphur isotope data are similar to isotopic determinations for other S-bearing phenocryst phases and glasses (Rye *et al.*, 1984; Cavarretta & Lombardi, 1990; Imai *et al.*, 1993; Luhr & Logan, 2002) for which a magmatic origin has been suggested. The euhedral character of the nosean phenocrysts in the Granadilla pumices, and their inclusion in other silicate phases (mainly feldspar) indicate magmatic crystallization in preference to the entrainment of xenocrysts. The high sulphur contents (Fig. 13) and

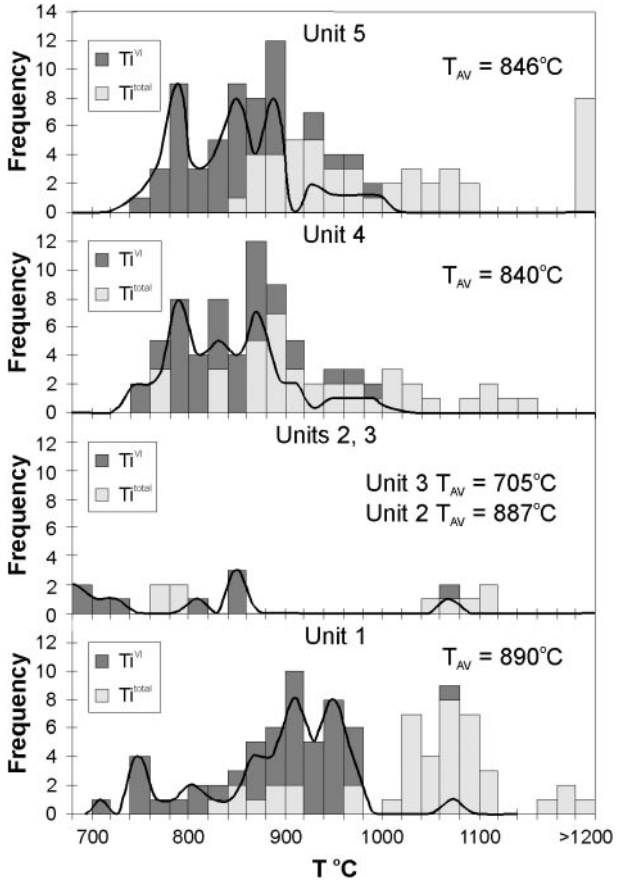


**Fig. 17.** Histogram of temperatures estimated from the biotite geothermometer of Luhr *et al.* (1984). Calculations based on the total content of Ti yield anomalously high temperatures, but recalculation using $Ti^{VI}$ yields temperature estimates in better agreement with Fe–Ti oxide thermometry. Temperature distribution curves and average temperatures ($T_{AV}$), based on $Ti^{VI}$, are also shown, and reinforce the stratigraphic variation of Fe–Ti geothermometry in which hotter phonolitic magma was erupted at the onset of the eruption, whereas the lowest temperature magma was erupted during the main plinian phase (Units 3–5).

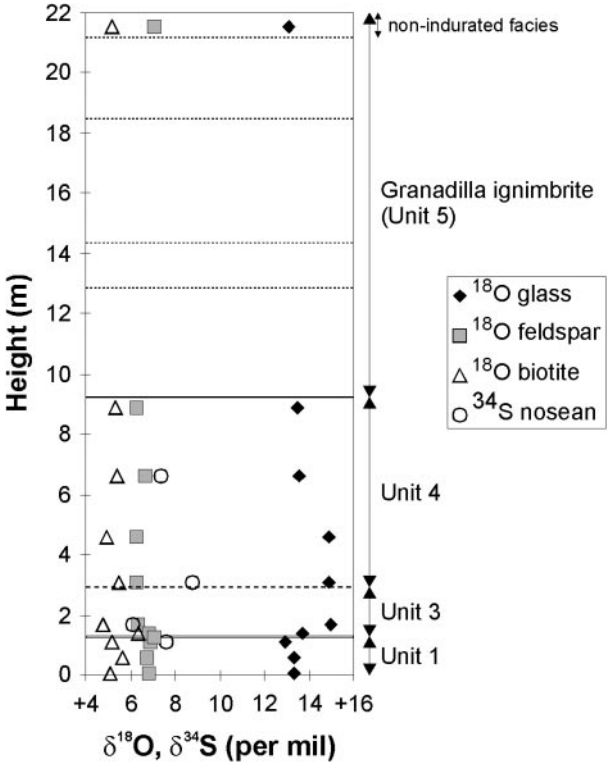


**Fig. 18.** Oxygen and sulphur isotopic compositions of mineral and glass separates vs stratigraphic height. The slight shift in isotopic composition above and below Unit 2 should be noted (grey bar).

magmatic isotopic compositions of the nosean phenocrysts, and the elevated $SO_3$ contents in apatites (see Pallister & Luhr, 1995; Fig. 15), coupled with the low $SO_3$ contents of phonolite pumice glasses, led Bryan *et al.* (2002) to conclude that: (1) the <1 Ma Las Cañadas phonolitic magmas coexisted with a separate $SO_2$-bearing gas phase (e.g. Wallace, 2001) that led to sulphur-rich explosive eruptions; and (2) basaltic underplating and gas sparging (Bachmann & Bergantz, 2003) were key processes responsible for maintaining an elevated abundance of sulphur (high $fSO_2$) in the phonolitic magma reservoir at shallow levels.

## DISCUSSION

### Petrogenesis

The phenocryst mineralogy and pumice chemistry of the Granadilla Member is similar to that of many other phonolite pyroclastic deposits on Tenerife (e.g. Wolff & Storey, 1984; Bryan *et al.*, 2002). However, the Granadilla eruption exhibited two unusual features: (1) a continuity and gradation in terms of minor and trace elements between the least and most evolved end-members without any abrupt or step-like changes; and (2) the tapping of hotter and more mafic magma during the opening phase of the plinian eruption, which resulted in a reverse then normal compositional and thermal zonation through the deposit.

As shown in previous studies, and supported by the new data presented here, the Granadilla Member exhibits a vertical chemical variation or 'cryptic zonation' (Wolff & Storey, 1984; Bryan *et al.*, 1998*a*). New analyses of juvenile pumice clasts show that this chemical variation is also expressed within the phenocryst assemblages, mineral chemistry, and corresponding intensive parameters (e.g. $T, fO_2, fH_2O$). Geothermometry estimates indicate that the major volume of phonolite magma possessed a gradient in temperature from 860 °C to ~790 °C (Fig. 16). Highest incompatible element abundances in pumice from the top of Unit 3 and base of Unit 4 (Fig. 3) confirm that this represents the most evolved portion of the phonolite magma. The ferromagnesian phases from these highly fractionated phonolite pumices are also

*Table 3: Water fugacity calculations and temperature and $fO_2$ estimates from coexisting Fe–Ti oxides*

| Sample | $T$(°C)* | log($fO_2$)* | $X$Fe$^{2+}$ | $X$OH | $a$san† | $X$Fe$_3$O$_4$ | log($f$H$_2$O) | $f$H$_2$O (bars)‡ |
|---|---|---|---|---|---|---|---|---|
| *Granadilla member* | | | | | | | | |
| 1i-1j | 800 | −14·1 | 0·37 | 0·81 | 0·56 | 0·69 | 2·72 | 520·25 |
| 8m | 800 | −14·1 | 0·35 | 0·8 | 0·62 | 0·65 | 2·56 | 365·49 |
| 6r | 800 | −14·2 | 0·31 | 0·84 | 0·57 | 0·66 | 2·44 | 275·6 |

*Temperature and $f$O2 estimates from coexisting Fe-Ti oxides.
†Sanidine activity based on the activity expression of Fuhrman & Lindsley (1988).
‡$f$(H$_2$O) in bars using the equation of Wones (1972).

*Table 4: Oxygen isotope data for glass, feldspar and biotite from the Granadilla Member*

| Sample | Lithology | Height (m) | Unit | Sample LOI | $\delta^{18}$O Glass | $\delta^{18}$O Feldspar | $\delta^{18}$O Biotite |
|---|---|---|---|---|---|---|---|
| *Granadilla Member* | | | | | | | |
| 6v | ignimbrite | 21·5 | 5 | 6·94 | 13·1 | 7·1 | 5·2 |
| 8q | pumice fallout | 8·9 | 4 | 6·76 | 13·5 | 6·3 | 5·3 |
| 8o | pumice fallout | 6·6 | 4 | 7·56 | 13·6 | 6·7 | 5·4 |
| 8m | pumice fallout | 4·6 | 4 | 7·77 | 14·9 | 6·3 | 5·0 |
| 8k | pumice fallout | 3·1 | 4 | 7·73 | 14·9 | 6·3 | 5·5 |
| 1i | pumice fallout | 1·55 | 3 | 8·48 | 15·0 | 6·4 | 4·8 |
| 111g | pumice fallout | 1·27 | 3 | 7·79 | 13·8 | 6·8 | 6·4 |
| 111f | phreatoplinian ash | 1·2 | 2 | — | — | 7·1 | — |
| 111e | pumice fallout | 1·17 | 1d | 7·55 | 13·0 | 6·9 | 5·2 |
| 111c | pumice fallout | 0·58 | 1c | 7·30 | 13·3 | 6·7 | 5·6 |
| 111a | pumice fallout | 0·08 | 1a | 7·05 | 13·3 | 6·8 | 5·1 |

Oxygen isotope results are in parts per thousand (per mil) relative to SMOW. Analyses were performed by Ms M. Jane at the Department of Earth Sciences, Monash University. 2σ errors are ±0·2‰.

correspondingly the most Fe-enriched, and key compatible minor and trace elements (e.g. Sr, Ba, $P_2O_5$, Ta, Sc) exhibit the strongest depletions (Fig. 3). The chemical variation through Units 3 to 5 was produced during the main plinian phase of the Granadilla eruption, when a buoyant and >25 km high eruption plume was established above a new vent (Bryan *et al.*, 2001). The main plinian phase of the Granadilla eruption, therefore, resembles many other large explosive eruptions producing compositionally zoned pyroclastic deposits [see the summary of examples given by Sumner & Wolff (2003)] where the withdrawal and eruption of a compositionally zoned chamber, and superposition have resulted in the inverse vertical compositional zonation (i.e. from most to least evolved) of the deposit.

Much of the cryptic chemical variation observed within the Granadilla Member can be accounted for by variable amounts of fractional crystallization (see Wolff, 1983; Wolff & Storey, 1984). Previous workers on Tenerife (e.g. Wolff & Storey, 1984; Ablay *et al.*, 1995) suggested sidewall crystallization as a viable process for generating the observed chemical gradients. Ablay *et al.* (1995) proposed a model of phonolite magma evolution by *in situ* fractionation (Chen & Turner, 1980; Langmuir, 1989) in which solidification occurs in a transition zone at the margins of the magma chamber. Residual liquid is then returned to the main convecting body of magma (Langmuir, 1989). One consequence of the *in situ* fractionation model is the generation of substantial variations in incompatible trace elements at essentially constant major element compositions, a feature consistent with observed elemental variations in the Granadilla Member (Fig. 3). There is no compelling evidence from petrographic features, mineral chemistry and stable isotope data (Table 4) to indicate that wall-rock assimilation (Wolff & Palacz, 1989) has been an important process in generating the geochemical characteristics of the Granadilla Member.

### *Magma mixing*

Although fractional crystallization has been important, the following petrographic evidence strongly supports the argument that magma mingling and mixing processes have also occurred, and that the effects of these processes have been superimposed on a phonolite magma evolving by *in situ* fractionation: (1) bimodal to polymodal phenocryst compositional populations (e.g. Figs 7 and 12); (2) the presence of both normally and reversely zoned phenocrysts (e.g. Fig. 8); (3) resorbed plagioclase in pumice clasts (Fig. 6b); and (4) quenched blebs of plagioclase- and hornblende-bearing microphenocrystic glass (Fig. 6a). Detailed analysis of the phenocryst phases has provided constraints on the petrological characteristics of the magmas involved in mixing. Magma mixing involved: (1) a dominant, highly evolved, thermally (860 to ~790 °C) and chemically zoned phonolite magma containing the phenocryst assemblage alkali feldspar + biotite + sodian diopside + titanite + Mg-poor titanomagnetite + Mg-poor ilmenite + nosean + apatite; and (2) a subordinate, hotter (>940 °C) tephriphonolitic magma containing the assemblage Ba-rich plagioclase feldspar (andesine-calcic anorthoclase) + kaersutite + diopside + Mg-rich titanomagnetite + Mg-rich ilmenite ± apatite ± nosean/haüyne. The latter mineralogy is particularly prevalent in pumices from Unit 1 and the

base of Unit 3. Despite the significant petrological differences, the two magmas must have been similar in overall major and minor element chemistry but differed substantially in some key minor and trace element abundances, notably Ba and Sr. Magma mixing is interpreted to have produced a hybrid melt that differed from the highly evolved end-member phonolite (e.g. as represented by pumice chemistry on either side of the Unit 3–4 contact) primarily in some minor and trace element abundances, primarily $TiO_2$, CaO, Ba, Sr and Zr (e.g. base of Unit 1, Fig. 3). Some of the anomalous bulk-pumice trace element abundances (e.g. Sr, Ba) also reflect the presence of Ba-rich plagioclase (e.g. Unit 1; Fig. 9) introduced by magma mixing. Magma mixing was incomplete, however, with quenched blebs of tephriphonolitic (Fig. 6a) magma present and evidence for mingling of the two melts (Fig. 6c) preserved. This process of magma mixing is very different from that recognized for almost all succeeding (<500 ka) phonolitic explosive eruptions from the Las Cañadas volcano, where the deposits contain abundant banded pumices reflecting magma mingling and mixing of phonolitic and phonotephritic–tephriphonolitic magmas, with the latter mafic magmatic component being the result of earlier magma mixing event(s) involving direct alkali basaltic magma input (Bryan *et al.*, 2002).

An important feature is that the occurrence of magma mingling or mixing features is related to stratigraphy, being most prevalent within Unit 1 (especially at the base), as well as in coarser pumice fall beds (Fig. 2). Mixed phenocryst populations (e.g. the co-occurrence of plagioclase and alkali feldspar and biotite with kaersutite) are associated with coarser pumice fall layers (e.g. subunit 1b—sample 111b; subunit 1d—sample 111d; Unit 4—sample 8n of Figs 7 and 8). The lack of normal zonation in the plagioclase phenocrysts from these coarser pumice fall layers (Fig. 8) is more consistent with syn-eruptive mingling of the two magma types, rather than pre-eruptive mixing when strong compositional zoning (e.g. samples 111a and 111g; Fig. 8) or dissolution would result. Magma mingling probably occurred in the conduit in response to periods of increased eruption vigour (i.e. increased discharge rates) that tapped larger and deeper zones of the magma chamber (e.g. Blake & Ivey, 1986a), or potentially during changes in vent location (e.g. base of Unit 3; Bryan *et al.*, 2001).

This raises the question of the origin of the reverse cryptic compositional zonation from the base to middle of the Granadilla pumice (Fig. 3), which is atypical of compositionally zoned pyroclastic rocks. The reverse zonation does not appear to reflect the tapping of less fractionated phonolite magma, similar to that represented by pumice at the top of the Granadilla Member (Fig. 4). Petrographic and mineral chemical data indicate that the pumice chemistry of Unit 1 has been modified by magma mixing, and some mingling of tephriphonolitic magma with phonolite. The gradation in pumice chemistry between the most evolved pumice compositions of Units 3 and 4 and the more mafic pumice compositions of Unit 1 may indicate that the hybrid magma produced by magma mixing may itself possess some compositional zonation that results from a decreasing proportion of the tephriphonolite magma component involved in mixing. This is supported by a relative decrease in the modal proportion of plagioclase in pumice clasts upwards through Unit 1 (Table 1). The highly evolved phonolite pumices from the main plinian fall Units 3 and 4 indicate that a substantial volume of the *in situ* fractionated phonolite magma remained largely unaffected by pre-eruptive mixing with tephriphonolite magma.

## Sr isotope disequilibrium

Variations in whole-rock $^{87}Sr/^{86}Sr$ ratios and the evidence that pumice glasses contain more radiogenic Sr than the bulk-pumices from the Granadilla eruption can be interpreted to indicate that either the melt and the phenocrysts were not in isotopic equilibrium at the time of eruption, or that post-eruptive alteration of the pumice glass has occurred, or both (Palacz & Wolff, 1989). Sr isotope disequilibrium has been identified in other large volume pyroclastic eruptions: e.g. Bishop Tuff (Halliday *et al.*, 1984; Christiansen & DePaolo, 1993), Bandelier Tuff (Wolff *et al.*, 1999), Whakamaru ignimbrites, Taupo (Brown *et al.*, 1998), and in the smaller volume, phonolitic Laacher See eruption (Wörner *et al.*, 1985, 1986). Any model for Sr isotopic variation in the Granadilla Member must account for the more radiogenic Sr isotope composition of the glass. Possible explanations for such glass–phenocryst isotopic disequilibrium are: (1) assimilation of radiogenic crustal material after the growth of the phenocrysts [assimilation plus fractional crystallization (AFC) processes]; (2) *in situ* decay of $^{87}Rb$ in a relatively high Rb/Sr melt (Christiansen & DePaolo, 1993); (3) post-eruptive alteration of hydrated pumice by meteoric water (Cousins *et al.*, 1993); and (4) syn-eruptive interaction between vesiculating magma and hydrothermal fluid (Palacz & Wolff, 1989).

Assimilation of more radiogenic crustal rocks in an AFC process can be discounted because: (1) Pb isotopes do not show any sympathetic variation with Sr isotopes (Palacz & Wolff, 1989); (2) assimilation would have to have occurred after feldspar crystallization; and (3) the samples in which contamination by wall-rock material may be identifiable (e.g. Unit 1) are also the least radiogenic in Sr. *In situ* ageing can be discounted because of the young age of the eruption (600 ka), the low Rb/Sr ratios (2–14), the potential time scales required ($>10^6$ yr), and that the last crystallizing phase (feldspar) shows no evidence of elevated Sr isotope ratios. Post-eruptive

alteration of the pumices was discounted by Palacz & Wolff (1989), who concluded that syn-eruptive interaction between magma and hydrothermal fluid was most likely to account for the observed Sr isotope disequilibrium between feldspar and glass. This model is an extension of that proposed by Wörner *et al.* (1985, 1986) for the Laacher See tephra. For the Granadilla eruption, such a model requires: (1) an active hydrothermal system at depth sourced from seawater (a suitable source of radiogenic strontium, $^{87}Sr/^{86}Sr$ ~0·709); (2) the wall-rock to the magma chamber to be dominated by hydrothermally altered and highly fractionated, low-Sr syenite; (3) hydrothermal fluid having access to the 'entire' magma reservoir, most likely to be at the conduit during eruption; (4) despite significant water interaction with magma, no change to the fragmentation or eruptive style (i.e. phreatomagmatic activity) occurred.

Some aspects of the Granadilla eruption indicate that syn-eruptive hydrothermal fluid interaction models are problematic, both for the Granadilla eruption and for the general application of the model to large plinian eruptions. First, lithic clast analysis for the Granadilla eruption (Bryan *et al.*, 2001) indicates that the accidental lithic assemblage is dominated by fresh, unaltered volcanic lithologies with altered syenite rare. Importantly, even for Unit 2, where there is clear evidence for water–magma interaction and a consequent change in the eruptive style (Bryan *et al.*, 2001), the lithic assemblage is predominantly fresh and unaltered. Second, 'flushing' of hydrothermal fluid through vesiculated magma on the scale required to enrich all pumice glass in radiogenic Sr would be expected to result in changes in eruptive behaviour and fragmentation processes (i.e. phreatic or phreatomagmatic activity). Where explosive eruptions are thought to have intersected hydrothermal systems (e.g. Mellors & Sparks, 1991), fundamental changes in eruption dynamics and erupted products (e.g. spatter agglomerates, increased lithic contents, lithic lag breccias and abundant evidence for phreatomagmatic volcanism) are observed. Although the phreatoplinian Unit 2 does record magma interaction at depth, the grain compositions and lithic assemblage are more consistent with magma interaction with an aquifer, rather than a hydrothermal system (Bryan *et al.*, 2001). No stratigraphic relationship between the phreatoplinian activity of Unit 2 and the enrichment of pumice glass in radiogenic Sr is apparent from the data of Palacz & Wolff (1989).

If hydrothermal fluid interaction is responsible for the Sr isotope disequilibrium, then this should be recorded by stable isotopes, as strong depletion in $^{18}O$ accompanies hydrothermal alteration of most rocks (Taylor & Sheppard, 1987; McConnell *et al.*, 1997; Bindeman *et al.*, 2001). The introduction of hydrothermal fluid or assimilation of hydrothermally altered wall-rock to cause the radiogenic Sr enrichment of the pumice glass should lead to a corresponding $\delta^{18}O$ depletion of the glasses from typical magmatic values. The high $\delta^{18}O$ values of glass (Table 4; Fig. 18) do not reflect high-temperature exchange with hydrothermal (meteoric or seawater-derived) fluids, but record a low-temperature exchange with meteoric water (e.g. Taylor, 1968; Halliday *et al.*, 1984). Supporting this is a positive correlation between $\delta^{18}O$ values and the LOI (an indicator of glass hydration) of the pumices (Table 4). The high $\delta^{18}O$ values of glass (Fig. 18) also indicate that all parts of the Granadilla deposit have been susceptible to post-eruptive modification. Cerling *et al.* (1985) demonstrated that hydration of silicic volcanic glass can be accompanied by oxygen isotope exchange resulting in an isotopic enrichment to >20‰, relative to SMOW. Although the Granadilla pumice remains largely fresh and unconsolidated, it has been modified and partly altered by secondary processes (Bryan *et al.*, 1998*a*). Calcite cement precipitated from groundwater is particularly evident in places (Bryan, 1998) and demonstrates the potential for hydration, alteration and low-temperature exchange with meteoric waters. The low Sr contents of the pumices (as low as 12 ppm; Table 2) make them particularly susceptible to Sr exchange. In contrast, the anomalously high Sr values for the Granadilla ignimbrite (124–186 ppm) reflect the mobility of Sr during vapour-phase alteration.

The introduction of radiogenic Sr into Sr-poor (≤40 ppm) pumice glass is alternatively attributed to groundwater flow, probably enriched in Sr by sea spray (e.g. Whipkey *et al.*, 2000), and subsequent hydration of pumice glass. The southern coast of Tenerife is affected daily by moderate to strong onshore sea breezes that deliver sea spray, which adheres to vegetation and the soil or rock surfaces until remobilized during rainfall events. Gislason & Eugster (1987) showed from the analysis of meteoric waters on Iceland that sea spray can be carried inland several tens of kilometres. Interpretations of the origin of radiogenic Sr disequilibrium between phenocryst phases and glass in pyroclastic deposits, particularly in oceanic island settings, should therefore be constrained by stable isotope analyses to evaluate the role of low-temperature exchange processes (see also Cousins *et al.*, 1993).

## Magma chamber configuration

The degree and nature of zonation of a pyroclastic deposit depends on the style of magma withdrawal from the magma chamber and eruption dynamics (e.g. Blake, 1981; Blake & Ivey, 1986*a*, 1986*b*). Zoned pyroclastic deposits typically grade from the most evolved compositions at the base to generally less evolved in the topmost parts, reflecting an inversion of a zoned magma chamber (e.g. Hildreth, 1979, 1981; Wolff & Storey, 1984; Wörner

& Schmincke, 1984*a*, 1984*b*; Druitt & Bacon, 1989). However, the reverse-to-normal cryptic zonation of the Granadilla Member (Fig. 3) argues that there was not a simple downward tapping of a zoned phonolite magma chamber (Wolff & Storey, 1984; Bryan *et al.*, 1998*a*). The vertical variations in mineralogy, Fe–Ti oxide composition and equilibrium temperatures, and pumice chemistry collectively suggest complexities in magma chamber configuration and/or magma withdrawal dynamics.

The following features need to be accounted for by the magma chamber configuration and/or withdrawal dynamics: (1) the withdrawal of hybridized phonolite magma at the start of the eruption, but with a systematic decrease in the proportion of the tephriphonolite component in successively erupted magma (i.e. the early phase of the eruption progressively tapped phonolite magma less affected by magma mixing); (2) a more regular drawdown of a zoned, highly fractionated phonolite magma during the main plinian phases (Units 3–5) that was essentially isolated from any magma mixing; and (3) a change in vent location between deposition of Units 1–2 and 3 (see Bryan *et al.*, 2001).

The hybrid characteristics of the first erupted magmas, and the incomplete mixing and preservation of disequilibrium textures, suggest that magma mixing occurred shortly prior to eruption. The presence of normal and reverse zoning in the feldspar and pyroxene phenocrysts (Figs 8 and 10) indicates that sufficient time occurred for crystallization to continue after the magmas became mixed. The gradual increase in incompatible, and decrease in compatible element abundances (Fig. 3), respectively, up sequence from Unit 1 to 3, indicates the increasing incorporation of phonolite magma unaffected by magma mixing. One possibility is that there is a mixed zone between zoned phonolite magma in the upper parts of the chamber, and underlying tephriphonolite (i.e. a three-layer stratified chamber configuration; e.g. Blake *et al.*, 1992). Minor and trace element variations of pumices upwards through Unit 1 would, therefore, reflect a compositional gradient in the mixed zone as a result of varying proportions of phonolite and tephriphonolite. However, such a simple layered configuration would require complex withdrawal dynamics to tap deeper levels (i.e. the mixed zone) of the chamber first. Alternatively, buoyant ascent of the hybrid magma may have established a conduit to the surface and thereby triggered the eruption (e.g. Pallister *et al.*, 1996). Hybridization and buoyant ascent could have been aided by a more vigorous episode of gas sparging (Bachmann & Bergantz, 2003) where the transfer and upward percolation of a hot gas phase was sufficient to disrupt the density interface between the cryptically zoned phonolite and underlying tephriphonolite. Gas sparging-triggered disturbance to the magma chamber may have been linked to mafic magma recharge at depth that did not penetrate the upper parts of the magma chamber.

The almost continuous vertical compositional and mineralogical variations through the main plinian fall units (Units 3 and 4; Fig. 3) argues against any major compositional gaps or abrupt compositional interfaces, and implies a pre-eruptive zonation of the phonolite in terms of composition (minor and trace element abundances), mineral chemistry, temperature and volatiles. The reappearance of kaersutite-phyric pumices at the top of the eruptive sequence in the Granadilla ignimbrite (Unit 5), coupled with the increase in Fe–Ti oxide temperature estimates, suggests that the zoned phonolitic capping layer was becoming exhausted, and the eruption began tapping deeper levels of the chamber. Because kaersutite and biotite do not co-precipitate in the Tenerife phonolites (see also Ablay *et al.*, 1998), the phonolite and tephriphonolite magma types are interpreted to have been separated by a compositional interface and density stratified.

Despite an eastwards shift in vent location of ~1·5 km (at the beginning of deposition of Unit 3; Bryan *et al.*, 2001), there is little indication of any abrupt change in magma chemistry, as illustrated by vertical chemical profiles through the Granadilla pumice (Fig. 3). Of significance is the coincidence in time between this shift in vent location and the more systematic draw-down of a more conventionally zoned phonolite magma (Units 3–5), where the effects of magma mixing were essentially absent. This suggests the possibility that the major volume of phonolite isolated from magma mixing was not in a geometrically simple vertical arrangement with 'mixed' phonolite magma, but that magma domains may have been laterally juxtaposed (e.g. Wilson & Hildreth, 1997).

A possible magma chamber configuration is outlined in Fig. 19. A large body of phonolite magma that developed by sidewall or *in situ* fractionation existed at the upper levels of a holding chamber, and possessed chemical, thermal and volatile gradients. Tephriphonolite magma occurred at depth and was separated from the overlying evolved phonolite magma by a density interface. The intrusion of tephriphonolite at a site along this interface promoted mixing with overlying phonolite to produce a hybrid magma differing primarily in minor and trace element abundances. The proportion of tephriphonolite involved in mixing decreased away from the mixing zone, producing both lateral and vertical chemical gradients between the magma end-members. Triggering of the eruption possibly resulted from the buoyant rise of the hybrid magma that then formed the first erupted products. Increasingly less contaminated phonolite magma was tapped as the eruption progressed, probably drawn in laterally to the conduit rather than from depth. However, during periods of increased discharge and eruption vigour, tephriphonolite or hybrid magma,

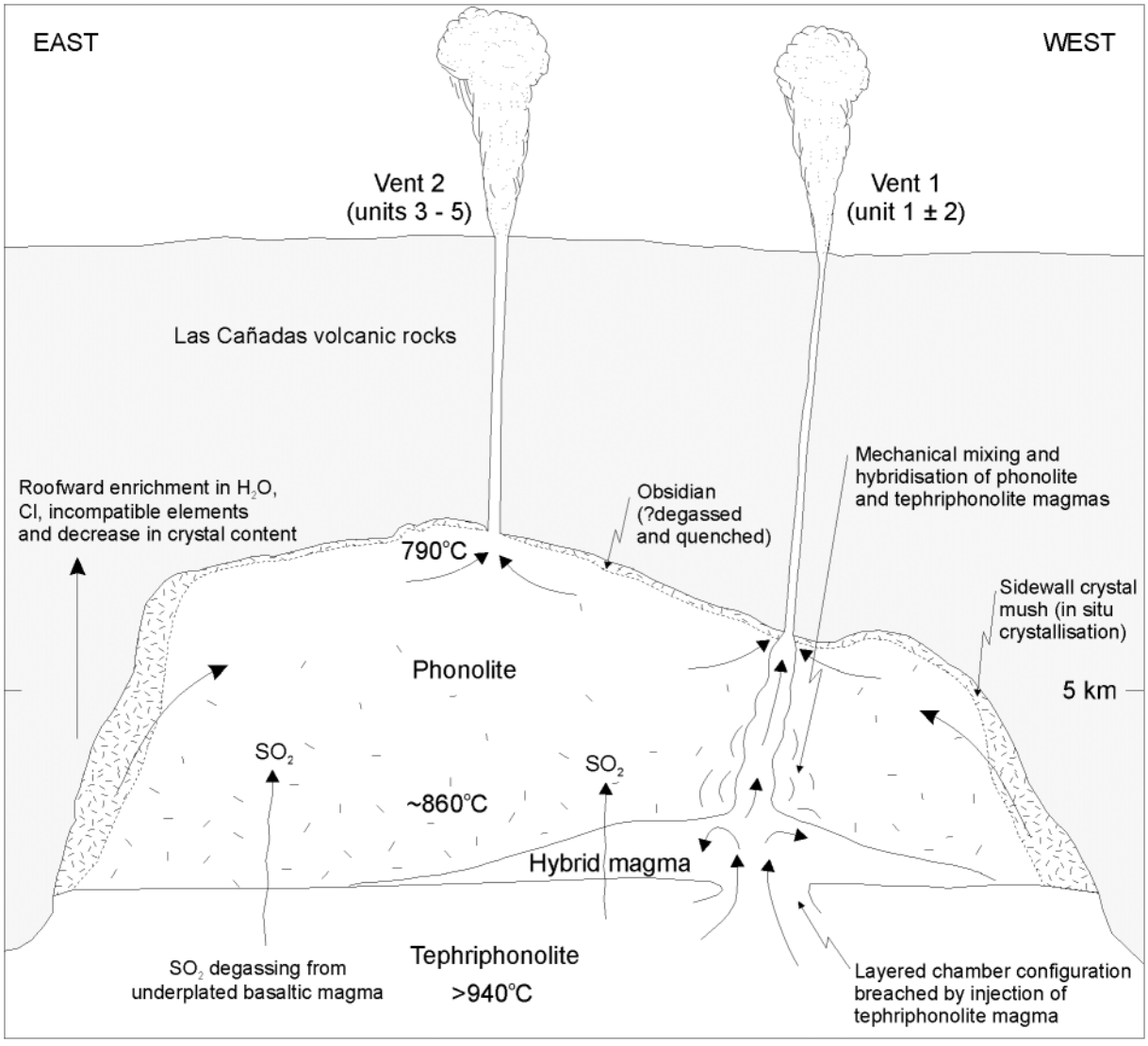


**Fig. 19.** Possible configuration of the Granadilla magma reservoir. The magma system consists of a large body of highly evolved phonolite magma developed by *in situ* (sidewall) fractional crystallization, which is underlain by tephriphonolite magma at depth. Intrusion of tephriphonolite magma promoted mingling and mixing, with a hybrid magma rising and venting at the onset of eruption (vent 1). The change in vent location as recorded by isopach and isopleth maps for Units 3 and 4 resulted in the more systematic withdrawal of highly evolved phonolite from vent 2, which had been isolated from magma mixing and mingling. Hybrid or tephriphonolitic magma partly gained access to the conduit during the main plinian phase from vent 2 when there were periods increased discharge and therefore a larger zone and depth of withdrawal.

probably occurring at deeper levels, was also tapped, as indicated by the correlation between bimodal mineral chemistry and coarse pumice fall beds. The change in vent location by the beginning of deposition of Unit 3 then tapped directly into the most evolved portion of the chamber reservoir, although banded pumices at the base of Unit 3 indicate some persistence of syn-eruptive mingling between the phonolite and hybrid or tephriphonolite magma. These pumices may alternatively represent a lag-time effect in plinian dispersal, such that there was a mixture of remnant pumice fallout sourced from vent 1, with pumice fallout derived from the new eruption plume developed at vent 2. Some indication for the contribution of fallout from more than one vent comes from the distinctive broadening and asymmetry of isopach contours for Unit 3 (Bryan *et al.*, 2001). Magma draw-down was then more regular during this main plinian phase of the Granadilla eruption.

The schematic model thus implies both vertical and lateral chamber zonation, in part caused by the vertical rise of hybrid magma. The eruptive sequence of hybrid followed by highly fractionated (or most evolved) magma was also observed, for example by Pallister *et al.* (1996), during the 1991 eruption of Pinatubo, where the first

eruptions were of hybrid andesite, followed by dacite during the main plinian phase. Those workers considered that the buoyant ascent of hybrid andesitic magma triggered the eruption. Consistent with this interpretation, other studies are increasingly recognizing that the simple, sequential tapping of a zoned magma chamber, from most to least evolved, is an oversimplification for several explosive eruptions (e.g. Freundt & Schmincke, 1992; Wilson & Hildreth, 1997; Brown *et al.*, 1998).

## CONCLUSIONS

The main conclusions from the petrology and geochemistry of the Granadilla Member are as follows.

(1) Major and trace element data and petrographic trends are consistent with a reverse-to-normal cryptic compositional zoning of the Granadilla Member. Cryptic zonation is interpreted to have developed in response to *in situ* (sidewall) fractionation (Chen & Turner, 1980; Langmuir, 1989). The reappearance of kaersutite-bearing pumice at the closing stages of the eruption (top of Granadilla ignimbrite) may indicate that the evolved phonolitic cap was exhausted, and the eruption began to tap deeper parts of the chamber. Trace element and REE data indicate the importance of the modal assemblage of alkali feldspar, apatite, Fe–Ti oxide, titanite and diopside as fractionating phases.

(2) Sulphur isotope data for nosean crystal separates are consistent with a magmatic origin for sulphur. Elevated $SO_3$ contents of apatites (up to 1 wt %), and the crystallization of nosean/haüyne over nepheline are interpreted as the result of the coexistence of a $SO_2$-bearing gas phase. Degassing from underlying basaltic magma is interpreted to have contributed to high $fSO_2$ in the overlying phonolitic cap, and possibly large $SO_2$ emissions on eruption.

(3) Oxygen isotope analyses of crystal and glass separates from pumices do not record hydrothermal fluid interaction with the vesiculating magma as the cause for Sr isotope disequilibrium between pumice glass and feldspar (see Palacz & Wolff, 1989). The heavy $\delta^{18}O$ values (+13 to +15‰) reflect post-eruptive low-temperature exchange between meteoric water (probably enriched in Sr by sea spray) and pumice glass. This is interpreted as the mechanism for introducing the radiogenic Sr into the pumice glass.

(4) Mixed phenocryst assemblages, the presence of both normally and reversely zoned and resorbed phenocrysts, and bimodal to divergent phenocryst populations suggest that magma mixing has been important in producing the geochemical characteristics of the early erupted phonolite magma. The occurrences of kaersutite, plagioclase, Mg–Al-rich titanomagnetite, Mg-rich ilmenite, and kaersutite-bearing mafic glass blebs within the basal fallout Units (1–3) are interpreted to record incomplete magma mixing just before eruption. The injection, mingling and mixing of tephriphonolitic magma may have led to eruption. The correlation of pumice within coarse pumice fallout beds containing a mixed phenocryst assemblage, however, suggests that hybrid or tephriphonolitic magma occurring at deeper levels was also tapped in response to eruption vigour.

(5) Fe–Ti oxide thermometry for the Granadilla Member indicates high eruptive temperatures at the onset of the eruption (~940 °C) that decreased to 800 °C through the main fallout phase (Unit 4), but increased to >900 °C during the emplacement of the Granadilla ignimbrite. Petrographic and geothermometry data indicate that the hotter, less evolved magma tapped at the start of the eruption was formed by mixing of phonolite and tephriphonolitic magma. The most evolved magma compositions (isolated from mixing) were tapped during the main plinian phases of the eruption (Units 3 and 4).

(6) Neither the vent migration pattern based on changes in vent location inferred from isopach maps for the constituent fall units (see Bryan *et al.*, 2001), the proportions and composition of juvenile clast types, nor the reverse-to-normal cryptic compositional zonation supports an oversimplified notion of an orderly drawdown of a geometrically simple, thermally and chemically stratified magma reservoir.

## ACKNOWLEDGEMENTS

Giray Ablay, Sylvia Zafrilla, Joan Martí, Ian Nicholls, Ian Cartwright, Ray Cas and John Clemens are thanked for valuable discussions on aspects of this paper. The foundation work of John Wolff has been instrumental in developing a new understanding of the Granadilla eruption in this study. The XRF analyses were performed by Frank Audsley, and ICP-MS analyses by Donna Korke. The support and assistance provided by Ron Rasch and David Cousins during microprobe sessions at the Centre for Microscopy & Microanalysis, University of Queensland, are gratefully acknowledged. This study formed part of PhD research at Monash University where S.B. was supported by an APA scholarship. S.B. has also been supported by the Damon Wells Fellowship at Yale University. A small ARC grant to Ray Cas assisted with some analytical costs. Field and technical support was provided by the Commission of the European Communities, DGXII, Environment Programme, Climatology and Natural Hazards Unit, in the framework of the contract EV5V-CT-0283, and by the DGICYT project PN-95-0002 to Joan Martí. Darren Chertkoff, Gerhard Wörner, John Wolff and especially Marjorie Wilson are thanked for their constructive reviews that greatly improved the manuscript.

## SUPPLEMENTARY DATA

Supplementary data for this paper are available at *Journal of Petrology* online.

## REFERENCES


Ablay, G. J., Ernst, G. G. J., Martí, J. & Sparks, R. S. J. (1995). The ~2 ka subplinian eruption of Montaña Blanca, Tenerife. *Bulletin of Volcanology* **57**, 337–355.

Ablay, G. J., Carroll, M. R., Palmer, M. R., Martí, J. & Sparks, R. S. J. (1998). Basanite–phonolite lineages of the Teide–Pico Viejo volcanic complex, Tenerife, Canary Islands. *Journal of Petrology* **39**, 905–936.

Albert-Beltran, J. F., Araña, V., Diez, J. L. & Valentin, A. (1990). Physical–chemical conditions of the Teide volcanic system (Tenerife, Canary Islands). *Journal of Volcanology and Geothermal Research* **43**, 321–332.

Ancochea, E., Fuster, J. M., Ibarrola, E., Cendrero, A., Coello, J., Hernan, F., Cantagrel, J. M. & Jamond, C. (1990). Volcanic evolution of the island of Tenerife (Canary Islands) in the light of new K–Ar data. *Journal of Volcanology and Geothermal Research* **44**, 231–249.

Bachmann, O. & Bergantz, G. W. (2003). Rejuvenation of the Fish Canyon magma body: a window into the evolution of large-volume silicic magma systems. *Geology* **31**, 789–792.

Bacon, C. R. & Hirschmann, M. M. (1988). Mg/Mn partitioning as a test for equilibrium between coexisting Fe–Ti oxides. *American Mineralogist* **73**, 57–61.

Bindeman I. N., Valley J. W., Wooden J. L. & Persing H. M. (2001). Post-caldera volcanism: *in situ* measurement of U–Pb age and oxygen isotope ratio in Pleistocene zircons from Yellowstone caldera. *Earth and Planetary Science Letters* **189**, 197–206.

Blake, S. (1981). Eruptions from zoned magma chambers. *Journal of the Geological Society, London* **138**, 281–287.

Blake, S. & Ivey, G. N. (1986*a*). Magma-mixing and the dynamics of withdrawal from stratified reservoirs. *Journal of Volcanology and Geothermal Research* **27**, 153–178.

Blake, S. & Ivey, G. N. (1986*b*). Density and viscosity gradients in zoned magma chambers, and their influence on withdrawal dynamics. *Journal of Volcanology and Geothermal Research* **30**, 201–230.

Blake, S., Wilson, C. J. N., Smith, I. E. M. & Walker, G. P. L. (1992). Petrology and dynamics of the Waimihia mixed magma eruption, Taupo Volcano, New Zealand. *Journal of the Geological Society, London* **149**, 193–207.

Bogaard, P. (1998). $^{40}Ar/^{39}Ar$ ages of Pliocene–Pleistocene fallout tephra units and volcaniclastic deposits in the sedimentary aprons of Gran Canaries and Tenerife (sites 953, 954 and 956). In: Weaver, P. P. E., Schmincke, H.-U., Firth, J. V. & Duffield, W. (eds) *Proceedings of the Ocean Drilling Program, Scientific Results, 157*. College Station, TX: Ocean Drilling Program, 329B41.

Booth, B. (1973). The Granadilla Pumice deposit of southern Tenerife, Canary Islands. *Proceedings of the Geological Association* **84**, 353–370.

Brown, R. J., Barry, T. L., Branney, M. J., Pringle, M. S. & Bryan, S. E. (2003). The Quaternary pyroclastic succession of southeast Tenerife, Canary Islands: explosive eruptions, related caldera subsidence, and sector collapse. *Geological Magazine* **140**, 265–288.

Brown, S. J. A., Wilson, C. J. N., Cole, J. W. & Wooden, J. (1998). The 340 ka Whakamaru-group ignimbrites, Taupo Volcanic Zone, New Zealand: geochemical evidence for non-sequential tapping of a zoned silicic magmatic system. *Journal of Volcanology and Geothermal Research* **84**, 1–37.

Bryan, S. E. (1998). Volcanology and petrology of the Granadilla Member, Tenerife (Canary Islands): constraints on the eruption dynamics, ignimbrite emplacement and caldera evolution. Ph.D. thesis, Monash University, Clayton, Vic., 632pp.

Bryan, S. E., Martí, J. & Cas, R. A. F. (1998*a*). Stratigraphy of the Bandas del Sur Formation: an extracaldera record of Quaternary phonolitic explosive eruptions from the Las Cañadas edifice, Tenerife (Canary Islands). *Geological Magazine* **135**, 605–636.

Bryan, S. E., Cas, R. A. F. & Martí, J. (1998*b*) Lithic breccias in intermediate volume phonolitic ignimbrites, Tenerife (Canary Islands): constraints on pyroclastic flow depositional processes. *Journal of Volcanology and Geothermal Research* **81**, 269–296.

Bryan, S. E., Cas, R. A. F. & Martí, J. (2001). The 0·57 Ma plinian eruption of the Granadilla Member, Tenerife (Canary Islands): an example of complexity in eruption dynamics and evolution. *Journal of Volcanology and Geothermal Research* **103**, 209–238.

Bryan, S. E., Martí, J. & Leosson, M. (2002). Petrology and geochemistry of the Bandas del Sur Formation, Las Cañadas edifice, Tenerife (Canary Islands). *Journal of Petrology* **43**, 1815–1856.

Carmichael, I. S. E. (1967). The iron–titanium oxides of salic volcanic rocks and their associated ferromagnesian silicates. *Contributions to Mineralogy and Petrology* **14**, 36–64.

Carmichael, I. S. E., Nicholls, J. & Smith, A. L. (1970). Silica activity in igneous rocks. *American Mineralogist* **55**, 246–263.

Cavaretta, G. & Lombardi, G. (1990). Origin of sulphur in the Quaternary perpotassic melts of Italy: evidence from haüyne sulphur isotope data. *Chemical Geology* **82**, 15–20.

Cerling, T. E., Brown, F. H. & Bowman, J. R. (1985). Low-temperature alteration of volcanic glass: hydration, Na, K, $^{18}O$ and Ar mobility. *Chemical Geology* **52**, 281–293.

Chen, C. F. & Turner, J. S. (1980). Crystallisation in a double-diffusive system. *Journal of Geophysical Research* **85**, 2573–2593.

Christiansen, J. N. & DePaolo, D. J. (1993). Time scales of large volume silicic magma systems: Sr isotopic systematics of phenocrysts and glass from the Bishop Tuff, Long Valley, California. *Contributions to Mineralogy and Petrology* **113**, 100–114.

Clayton, R. & Mayeda, T. K. (1963). The use of bromine pentafluoride in the extraction of oxygen from oxides and silicates for isotopic analysis. *Geochimica et Cosmochimica Acta* **27**, 43–52.

Cousins, B. L., Spera, F. J. & Dobson, P. F. (1993). Post-eruptive alteration of silicic ignimbrites and lavas, Gran Canaries, Canary Islands: strontium, neodymium, lead, and oxygen isotopic evidence. *Geochimica et Cosmochimica Acta* **57**, 631–640.

Druitt, T. H. & Bacon, C. R. (1989). Petrology of the zoned calc-alkaline magma chamber of Mount Mazama, Crater Lake, Oregon. *Contributions to Mineralogy and Petrology* **101**, 245–259.

Edgar, C. J., Wolff, J. A., Nichols, H. J., Cas, R. A. F. & Martí, J. (2002). A complex Quaternary ignimbrite-forming phonolitic eruption; the Poris Member of the Diego Hernandez Formation (Tenerife, Canary Islands). *Journal of Volcanology and Geothermal Research* **118**, 99–130.

Freundt, A. & Schmincke, H.-U. (1992). Mixing of rhyolite, trachyte and basalt magma erupted from a vertically and laterally zoned reservoir, composite flow P1, Gran Canaries. *Contributions to Mineralogy and Petrology* **112**, 1–19.

Fuhrman, M. L. & Lindsley, D. H. (1988). Ternary-feldspar modelling and thermometry. *American Mineralogist* **73**, 210–215.

Fuster, J. M., Araña, V., Brandle, J. L., Navarro, M., Alonso, U. & Aparcio, A. (1968). *Geologia y Volcanogia de Las Islas Canarias: Tenerife*. Madrid: Instituto 'Lucas Mallada', CSIC, 218 pp.

Ghiorso, M. S. & Sack, R. O. (1991). Fe–Ti oxide geothermometry: thermodynamic formulation and the estimation of intensive

variables in silicic magmas. *Contributions to Mineralogy and Petrology* **108**, 485–510.

Gislason, S. R. & Eugster, H. P. (1987). Meteoric water–basalt interactions. II: A field study in N.E. Iceland. *Geochimica et Cosmochimica Acta* **51**, 2841–2855.

Halliday, A. N., Fallick, A. E., Hutchinson, J. & Hildreth, W. (1984). A Nd, Sr and O isotopic investigation into the causes of chemical and isotopic zonation in the Bishop Tuff, California. *Earth and Planetary Science Letters* **68**, 379–391.

Harmon, R. S. & Hoefs, J. (1995). Oxygen isotope heterogeneity of the mantle deduced from global $^{18}O$ systematics of basalts from different geotectonic settings. *Contributions to Mineralogy and Petrology* **120**, 95–114.

Higgins, J. B. & Ribbe, P. H. (1976). The crystal chemistry and space groups of natural and synthetic titanites. *American Mineralogist* **61**, 878–888.

Hildreth, W. (1979). The Bishop Tuff: evidence for the origin of compositional zonation in silicic magma chambers. In: Chapin, C. E. & Elston, W. E. (eds) *Ash-flow Tuffs. Geological Society of America Special Paper* **180**, 43–75.

Hildreth, W. (1981). Gradients in silicic magma chambers: implications for lithospheric magmatism. *Journal of Geophysical Research* **86**, 10153–10192.

Hildreth, W. & Mahood, G. A. (1985). Correlation of ash-flow tuffs. *Geological Society of America Bulletin* **96**, 968–974.

Imai, A., Listanco, E. L. & Fujii, T. (1993). Petrologic and sulfur isotopic significance of highly oxidised and sulfur-rich magma of Mt. Pinatubo, Philippines. *Geology* **21**, 699–702.

Jones, A. P. (1984). Mafic silicates from the nepheline syenites of the Motzfeldt centre, South Greenland. *Mineral Magazine* **346**, 1–12.

Langmuir, C. H. (1989). Geochemical consequences of *in situ* crystallisation. *Nature* **340**, 199–205.

Lessing, P. & Grout, C. M. (1971). Haüynite from Edwards, New York. *American Mineralogist* **56**, 1096–1100.

Lipman, P. W. (1971). Iron–titanium oxide phenocrysts in compositionally zoned ash-flow sheets from southern Nevada. *Journal of Geology* **79**, 438–456.

Loferski, P. J. & Ayuso, R. A. (1991). Petrography and mineral chemistry of the composite Deboullie pluton, northern Maine, U.S.A.: implications for the genesis of Cu–Mo mineralisation. *Chemical Geology* **123**, 89–105.

Luhr, J. F. & Logan, M. A. V. (2002). Sulfur isotope systematics of the 1982 El Chichón trachyandesite: an ion microprobe study. *Geochimica et Cosmochimica Acta* **66**, 3303–3316.

Luhr, J. F., Carmichael, I. S. E. & Varecamp, J. C. (1984). The 1982 eruptions of El Chichón volcano, Chiapas, Mexico: mineralogy and petrology of the anhydrite-bearing pumices. *Journal of Volcanology and Geothermal Research* **23**, 69–108.

Martí, J., Mitjavila, J. & Araña, V. (1994). Stratigraphy, structure and geochronology of the Las Cañadas caldera (Tenerife, Canary Islands). *Geological Magazine* **131**, 715–727.

McConnell, V. S., Valley, J. W. & Eichelberger, J. C. (1997). Oxygen isotope compositions of intracaldera rocks: hydrothermal history of the Long Valley Caldera, California. *Journal of Volcanology and Geothermal Research* **76**, 83–109.

Mellors, R. A. & Sparks, R. S. J. (1991). Spatter-rich pyroclastic flow deposits on Santorini, Greece. *Bulletin of Volcanology* **53**, 327–342.

Morimoto, M., Fabries, J., Ferguson, A. K., Ginzburg, I. V., Ross, M., Seifert, F. A., Zussman, J., Aoki, K. & Gottardi, G. (1988). Nomenclature of pyroxenes. *Mineralogical Magazine* **52**, 535–550.

Munoz, J. L. (1984). F–OH and Cl–OH exchange in micas with applications to hydrothermal ore deposits. In: Bailey, S. W. (ed.) *Micas. Mineralogical Society of America, Reviews in Mineralogy* **13**, 469–493.

Neilsen, C. H. & Sigurdsson, H. (1981). Quantitative methods for electron microprobe analysis of sodium natural and synthetic glasses. *American Mineralogist* **66**, 547–552.

Norrish, K. & Hutton, J. T. (1969). An accurate X-ray spectrographic method for the analysis of a wide range of geological samples. *Geochimica et Cosmochimica Acta* **33**, 431–453.

Palacz, Z. A. & Wolff, J. A. (1989). Strontium, neodynium and lead isotope characteristics of the Granadilla pumice, Tenerife: a study of the causes of strontium isotope disequilibrium in felsic pyroclastic deposits. In: Saunders, A. D. & Norry, M. J. (eds) *Magmatism in the Ocean Basins. Geological Society, London, Special Publications* **42**, 147–159.

Pallister, J. S. & Luhr, J. F. (1995). Recognising ancient sulfur-rich eruptions: lessons from Pinatubo, El Chichón and Mount St. Helens. *International Union of Geodesy and Geophysics, XXI General Assembly, Boulder, CO*, A279.

Pallister, J. S., Hoblitt, R. P., Meeker, G. P., Knight, R. J. & Siems, D. F. (1996). Magma mixing at Mount Pinatubo: petrographic and chemical evidence from the 1991 deposits. In: Newhall, C. G. & Punongbayan, R. S. (eds) *Fire and Mud: Eruptions and Lahars of Mount Pinatubo, Philippines*. Seattle, WA: University of Washington Press, pp. 687–731.

Pérez-Torrado, F. J., Martí, J., Queralt, I. & Mangas, J. (1995). Alteration processes of the Roque Nublo ignimbrites (Gran Canaries, Canary Islands). *Journal of Volcanology and Geothermal Research* **65**, *191–204*.

Rutherford, M. J. (1993). Experimental petrology applied to volcanic processes. *EOS Transactions, American Geophysical Union* **74**, 49, 55.

Rye, R. O., Luhr, J. F. & Wasserman, M. D. (1984). Sulfur and oxygen isotopic systematics of the 1982 eruptions of El Chichón volcano, Chiapas, Mexico. *Journal of Volcanology and Geothermal Research* **12**, 109–123.

Schneiderman, J. S. (1991). Petrology and mineral chemistry of the Ascutney Mountain igneous complex. *American Mineralogist* **76**, 218–229.

Scott, P. W. (1976). Crystallisation trends of pyroxenes from the alkaline volcanic rocks of Tenerife, Canary Islands. *Mineralogical Magazine* **40**, 805–816.

Sparks, R. S. J. (1978). The dynamics of bubble formation and growth in magmas: a review and analysis. *Journal of Volcanology and Geothermal Research* **3**, 1–37.

Stormer, J. C. & Carmichael, S. E. (1971). The free energy of sodalite and the behavior of chloride, fluoride and sulfate in silicate magmas. *American Mineralogist* **56**, 292–306.

Sumner, J. M. & Wolff, J. A. (2003). Petrogenesis of mixed-magma, high-grade, peralkaline ignimbrite 'TL' (Gran Canaries): diverse styles of mixing in a replenished, zoned magma chamber. *Journal of Volcanology and Geothermal Research* **126**, 109–126.

Taylor, H. P. (1968). The oxygen isotope geochemistry of igneous rocks. *Contributions to Mineralogy and Petrology* **19**, 1–71.

Taylor, H. P. & Sheppard, S. M. F. (1987). Igneous rocks: I. Processes of isotopic fractionation and isotope systematics. In: Valley, J. W., Taylor, H. P. & O'Neil, J. R. (eds) *Stable Isotopes in High Temperature Geological Processes. Mineralogical Society of America, Reviews in Mineralogy* **16**, 165–184.

Thirlwall, M. F., Singer, B. S. & Marriner, G. F. (2000). $^{39}Ar$–$^{40}Ar$ ages and geochemistry of the basaltic shield stage of Tenerife, Canary Islands, Spain. *Journal of Volcanology and Geothermal Research* **103**, 247–297.

Thomas, N., Jaupart, C. & Vergniolle, S. (1994). On the vesicularity of pumice. *Journal of Geophysical Research* **99**, 15633–15644.

Valentin, A., Albert-Beltran, J. F. & Diez, J. L. (1990). Geochemical and geothermal constraints on magma bodies associated with

historic activity, Tenerife (Canary Islands). *Journal of Volcanology and Geothermal Research* **44**, 251–264.

Walker, G. P. L. (1972). Crystal concentration in ignimbrites. *Contributions to Mineralogy and Petrology* **36**, 135–146.

Wallace, P. J. (2001). Volcanic $SO_2$ emissions and the abundance and distribution of exsolved gas in magma bodies. *Journal of Volcanology and Geothermal Research* **108**, 85–106.

Whipkey, C. E., Capo, R. C., Chadwick, O. A. & Stewart, B. W. (2000). The importance of sea spray to the cation budget of a coastal Hawaiian soil: a strontium isotope approach. *Chemical Geology* **168**, 37–48.

Wilson, C. J. N. & Hildreth, W. (1997). The Bishop Tuff: new insights from eruptive stratigraphy. *Journal of Geology* **105**, 407–439.

Wolff, J. A. (1983). Petrology of Quaternary pyroclastic deposits from Tenerife, Canary Islands. Ph.D. thesis, University of London, London, 542 pp.

Wolff, J. A. (1984). Variation in Nb/Ta during differentiation of phonolitic magma, Tenerife, Canary Islands. *Geochimica et Cosmochimica Acta* **48**, 1345–1348.

Wolff, J. A. (1985). The effect of explosive eruption processes on geochemical patterns within pyroclastic deposits. *Journal of Volcanology and Geothermal Research* **26**, 189–201.

Wolff, J. A. & Palacz, Z. A. (1989). Pb isotope and trace-element variation in the phonolitic Granadilla Series, Tenerife: evidence for recycling within an ocean island volcano. *Mineralogical Magazine* **53**, 519–525.

Wolff, J. A. & Storey, M. (1983). The volatile component of some pumice-forming alkaline magmas from the Azores and Canary Islands. *Contributions to Mineralogy and Petrology* **82**, 66–74.

Wolff, J. A. & Storey, M. (1984). Zoning in highly alkaline magma bodies. *Geological Magazine* **121**, 563–575.

Wolff, J. A., Ramos, F. C. & Davidson, J. P. (1999). Sr isotope disequilibrium during differentiation of the Bandelier Tuff; constraints on the crystallisation of a large rhyolitic magma chamber. *Geology* **27**, 495–499.

Wones, D. R. (1972). Stability of biotite: a reply. *American Mineralogist* **57**, 316–317.

Wörner, G. & Schmincke, H.-U. (1984a) Mineralogical and chemical zonation of the Laacher See tephra sequence (East Eifel, W. Germany). *Journal of Petrology* **25**, 805–835.

Wörner, G. & Schmincke, H.-U. (1984b) Petrogenesis of the zoned Laacher See Tephra. *Journal of Petrology* **25**, 836–851.

Wörner, G., Staudigel, H. & Zindler, A. (1985). Isotopic constraints on open system evolution of the Laacher See magma chamber (Eifel, West Germany). *Earth and Planetary Science Letters* **75**, 37–49.

Wörner, G., Harmon, R. S. & Hoefs, J. (1986). Stable isotope relations in an open magma system, Laacher See, Eifel (F.R.G.). *Contributions to Mineralogy and Petrology* **95**, 343–349.